NASA TN D-1032

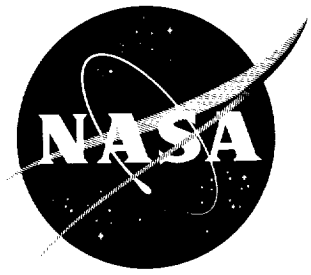

TECHNICAL NOTE

D-1032

STOL CHARACTERISTICS OF A PROPELLER-DRIVEN, ASPECT-RATIO-10, STRAIGHT-WING AIRPLANE WITH BOUNDARY-LAYER CONTROL FLAPS, AS ESTIMATED FROM LARGE-SCALE WIND-TUNNEL TESTS

By James A. Weiberg and Curt A. Holzhauser

Ames Research Center
Moffett Field, Calif.

NATIONAL AERONAUTICS AND SPACE ADMINISTRATION

WASHINGTON

June 1961

1Z

NATIONAL AERONAUTICS AND SPACE ADMINISTRATION

TECHNICAL NOTE D-1032

STOL CHARACTERISTICS OF A PROPELLER-DRIVEN, ASPECT-RATIO-10, STRAIGHT-WING AIRPLANE WITH BOUNDARY-LAYER CONTROL FLAPS, AS ESTIMATED FROM LARGE-SCALE WIND-TUNNEL TESTS

By James A. Weiberg and Curt A. Holzhauser

SUMMARY

A study is presented of the improvements in take-off and landing distances possible with a conventional propeller-driven transport-type airplane when the available lift is increased by propeller slipstream effects and by very effective trailing-edge flaps and ailerons. This study is based on wind-tunnel tests of a 45-foot span, powered model, with BLC on the trailing-edge flaps and controls. The data were applied to an assumed airplane with four propellers and a wing loading of 50 pounds per square foot. Also included is an examination of the stability and control problems that may result in the landing and take-off speed range of such a vehicle.

The results indicated that the landing and take-off distances could be more than halved by the use of highly effective flaps in combination with large amounts of engine power to augment lift (STOL). At the lowest speeds considered (about 50 knots), adequate longitudinal stability was obtained but the lateral and directional stability were unsatisfactory. At these low speeds, the conventional aerodynamic control surfaces may not be able to cope with the forces and moments produced by symmetric, as well as asymmetric, engine operation. This problem was alleviated by BLC applied to the control surfaces.

INTRODUCTION

Interest in obtaining short take-off and landing (STOL) performance led to the wind-tunnel tests of a large-scale propeller-driven transport-type model reported in references 1 to 4. Boundary-layer control (BLC) applied to trailing-edge flaps and ailerons provided large increases in lift because of the increased effectiveness of the flap in the propeller slipstream. However, the data were not presented in terms of STOL performance improvements possible, nor were the limitations pointed out. Subsequent to the wind-tunnel tests, flight experience was obtained with an airplane similar to the model of reference 2. Some of the problems that resulted when STOL-type approaches and landings were made are reported in reference 5.

The present report is an analysis of the data of references 1 to 4 and previously unreported data to show the extent to which these high lift coefficients can be utilized to obtain STOL performance of a conventional propeller-driven transport-type airplane of moderate thrust. Also included is an examination of the stability and control problems that result at these low speeds and moderate thrust values. Pertinent points of the flight tests (ref. 5) are also noted in relation to the wind-tunnel results. When possible, methods to alleviate the problem areas are given.

NOTATION

A 4 2 3

b	wing span, ft
$\bar{c}$	mean aerodynamic chord, $\frac{2}{S}\int_0^{b/2} c^2 dy$, ft
C_D	drag coefficient including thrust, $\frac{\text{measured drag}}{qS}$
C_D'	drag coefficient,[1] $C_D + T_c'$
C_L	lift coefficient, $\frac{\text{lift}}{qS}$
C_{L_t}	horizontal-tail lift coefficient, $\frac{\text{horizontal-tail lift}}{qS_t}$
C_l	rolling-moment coefficient, $\frac{\text{rolling moment}}{qSb}$
C_{l_p}	damping in roll, $\frac{\partial C_l}{\partial(pb/2V)}$, per radian
C_m	pitching-moment coefficient, $\frac{\text{pitching moment}}{qS\bar{c}}$
C_{m_α}	attitude stability parameter, $\frac{\partial C_m}{\partial \alpha}$, per deg; V, T_c', δ_e held constant
C_{m_V}	speed stability parameter, $\frac{\partial C_m}{\partial V}$, per fps; α, power, δ_e held constant
C_n	yawing-moment coefficient, $\frac{\text{yawing moment}}{qSb}$

[1] With the usual notation, positive thrust is in the negative drag direction.

C_Q flow coefficient, $\frac{w_a}{\rho g V S}$

C_Y side-force coefficient, $\frac{\text{side force}}{qS}$

C_{n_β}, C_{l_β}, C_{Y_β} slopes of curves of C_n, C_l, and C_Y vs. β measured at $\beta = 0$, per deg

A 4 2 3

C_μ blowing momentum coefficient, $\frac{w_a}{gqS} V_j$ or $\frac{w_a}{gqS_t} V_j$

D drag, lb

h_j nominal height of blowing nozzle, ft

I_x, I_y, I_z moments of inertia about x, y, and z axis

i_t horizontal-tail incidence, deg

L lift, lb

L_p $\frac{qSb^2}{2VI_x} C_{l_p}$, per sec

p rate of rolling, radians/deg

$\frac{pb}{2V}$ wing tip helix angle in roll, radians

P_d duct pressure coefficient, difference between duct and free-stream static pressures divided by free-stream dynamic pressure

g acceleration of gravity, 32.2 ft/sec^2

q free-stream dynamic pressure, lb/sq ft

s distance, ft

S wing area, sq ft

S_t horizontal-tail surface area, sq ft

T total thrust, lb

T_o	total thrust at zero velocity, lb
T_c'	thrust coefficient, $\frac{T}{qS}$
V	free-stream velocity, fps or k
V_j	jet velocity assuming isentropic expansion (see ref. 4)
V_s	stall speed, k
W	gross weight, lb
w_a	air-flow rate, lb/sec
x	distance from $\bar{c}$ leading edge to center of gravity parallel to fuselage reference line, ft
y	spanwise distance perpendicular to plane of symmetry, ft
z	vertical distance from thrust line perpendicular to fuselage reference line, ft; positive down
α	angle of attack, deg
β	angle of sideslip, deg
γ	climb or glide angle, deg or radians
δ	deflection of movable surface, deg
ζ	damping ratio
$\ddot{\theta}$	initial angular acceleration in pitch, $\frac{C_m q S \bar{c}}{I_y}$, radians/sec^2
μ	friction coefficient
ρ	mass density of air, slugs/cu ft
τ	roll time constant, $\frac{-1}{I_p}$, sec
$\ddot{\varphi}$	initial angular acceleration in roll, $\frac{C_l S b}{I_x}$, radians/sec^2
ω_n	undamped natural frequency, cps

Subscripts

a aileron

e elevator

f flap

n nose

A
4
2
3 r rudder

t horizontal tail

MODEL AND ASSUMED AIRPLANE

The analysis presented is primarily based on tests of a model representative of a four-propeller transport-type airplane with a straight wing of aspect ratio 10. This model had blowing BLC over the flaps and ailerons (ref. 4). The model is shown installed in the Ames 40- by 80-Foot Wind Tunnel in figure 1(a) and the geometry is given in figure 1(b) and table I. Details of the trailing-edge flaps and ailerons are shown in figure 1(c). The details of the horizontal tail modified for blowing on a leading-edge flap and over the elevator are presented in figure 1(d).

In addition to the data on the four-propeller model, a limited amount of data from tests of a two-propeller model is used in the analysis. This two-propeller version had the same total disk area as the four-propeller model. (Right-hand-rotation propellers were used on both models.) The two-propeller model was tested with a combination slot-suction and blowing flaps and blowing ailerons (Arado system reported in ref. 1), with area suction on the flaps and ailerons (ref. 2), and with blowing over the flaps and ailerons (ref. 3).

Additional information pertaining to the models and details of the propeller geometry and characteristics may be found in references 1, 2, 3, and 4.

For purposes of the analysis, an airplane with a wing loading of 50 pounds per square foot and a gross weight of 61,800 pounds has been assumed. The physical characteristics of this airplane are similar to those of the flight vehicle (ref. 5) and are given in table II.

TESTS AND CORRECTIONS

The tests reported in references 2, 3, and 4 were made at free-stream velocities from 51 to 93 feet per second (q of 3 to 10 lb/sq ft), corresponding to Reynolds numbers of 1.4 to 2.6 million based on the mean aerodynamic chord of the model. The propeller thrust calibration was made with the flaps and ailerons undeflected and with the model set at an angle of attack for zero lift. Propeller shaft thrust was not measured directly; therefore, it was assumed that the propeller thrust was equal to the sum of the measured thrust and the measured drag of the model with the propellers removed. For setting thrust coefficient during a run, the propeller rotational speed was held constant, and it was assumed that there was no variation of thrust with either angle of attack or upwash due to flap deflection.

A 4 2 3

Standard tunnel-wall corrections were applied to the data; these are detailed in the respective references. No corrections were made for strut tares or strut interference.

RESULTS AND DISCUSSION

The following analysis pertains to the landing and take-off performance of a propeller-driven transport and the stability and control problems that may arise in this speed range.

For this analysis a maximum deflection of 40° will be used on the flap without BLC, since larger deflections produced only small increases in lift. For comparative purposes, the maximum deflection of the flap with blowing BLC will be 80°. In addition, when BLC is applied to the ailerons, they may be drooped since reference 3 showed that the drooped ailerons with BLC could be deflected differentially and yet maintain an effectiveness as great as the undrooped ailerons without BLC. It is, of course, recognized that the lift increment produced by the single-slotted flap can be increased by means other than BLC, for example, by the use of chord-increasing double-slotted flaps. It would be expected that for such cases the results obtained would be between those presented without BLC and those with BLC.

The term STOL in this report shall be used in a manner similar to that in reference 6; that is, it shall refer to the regime of flight where engine power is used to augment the lift, thereby reducing the landing and take-off distances.

Landing and Take-Off Performance

Representative lift- and drag-coefficient data at various thrust coefficients are presented in figure 2 for the model without BLC ($\delta_f = 40^\circ$, $\delta_a = 0^\circ$) and with BLC ($\delta_f = 60^\circ$, $\delta_a = 30^\circ$). Two drag coefficients are shown. The center plot represents the measured drag coefficient with the thrust coefficient included. Here $C_D = 0$ indicates balance in level unaccelerated flight; negative C_D corresponds to climbing or accelerating flight; and positive C_D corresponds to sinking or decelerating flight. For unaccelerated flight $\tan^{-1}(C_D/C_L)$ corresponds to the glide angle γ. For level flight C_D/C_L corresponds to the deceleration in g's. The left-hand plot has the horizontal thrust component removed and is useful in indicating the approximate aerodynamic changes that result from increased thrust coefficient.

A 4 2 3

Approach speed and landing distance.- To obtain an indication of the reduction in landing speed and landing distance that may be possible by using very effective flaps in an STOL approach, it will be assumed that the pilot will approach and land at a speed 15 percent greater than the power-on stall speed. For comparative purposes, approach and landing at a speed 30 percent greater than the power-off stall speed shall also be examined. Such a landing represents the current conventional landing approach (ref. 7) where the lift due to thrust is not used. It is recognized that the approach speed chosen by a pilot can depend on factors other than stall speed (e.g., visibility, buffet, etc., as discussed in ref. 8). However, it is felt that stall speed based on $C_{L_{max}}$ can be used in this report as an indication of the relative gains possible.

In flight, the power-on approach and stall speeds would probably be evaluated at a constant setting of the engine controls. Consequently, the approach speed and hence approach C_L would not be determined in terms of stall speed or $C_{L_{max}}$ at a constant thrust coefficient, since T_c' will also change with speed for a constant engine control setting. The variation of T_c' with C_L will depend on the propeller characteristics and engine governing system. For the following analysis, it has been assumed that the propeller thrust does not vary over the speed range of interest. Hence, for a given power setting, T_c' varies linearly with C_L corresponding to a constant T/W. The approach speed for a given glide angle or descent rate in a power-on approach is conveniently determined from a cross plot of the data in the form of figure 3. In addition to the variation of $C_{L_{max}}$ with T_c' and C_L with C_D' for particular flight conditions, rays of constant thrust-to-weight ratios are shown. Therefore, if the approach speed is established in terms of $C_{L_{max}}$ (i.e., $1.15V_s$, power on), the approach C_L variation with T_c' is found by following lines of constant T/W. Knowledge of the C_D' at a given C_L and T_c' will then provide sufficient data to establish the glide angle or descent rate at the desired approach speed.

The foregoing method was used to obtain approach speeds at various glide angles for an airplane with a wing loading of 50 pounds per square foot. Values for these angles are presented in figure 4 along with the total landing distance over a 50-foot obstacle; these values were calculated by means of the equations and assumptions given in the appendix. Corresponding values of speed and distance for an airplane descending at a rate of 500 feet per minute are summarized in the following table:

			Conventional approach			STOL approach		
BLC	δ_f, deg	δ_a, deg	$C_{L_{max}}$	$1.3V_s$, power off, k (1)	Total landing distance, ft	$C_{L_{max}}$	$1.15V_s$, power on, k (1)	Total landing distance, ft
off	40	0	2.0	112	3100	2.6	86	1900
on	80	30	3.3	87	2100	6.1	58	1200

[1]Power required for 500 fpm rate of descent.

There are several points worthy of note in figure 4 and in the above table. One, of course, is the large reduction in approach speed and landing distance that results from the use of an effective trailing-edge flap when combined with the slipstream. For an STOL approach, the shortest flare and ground roll distances are obtained with an essentially flat approach (fig. 5); however, the air distance to clear an obstacle in the approach path is least for a steep approach. For the configurations examined, the shortest total landing distance was obtained at a relatively shallow glide angle. In contrast, for a conventional approach where slipstream effects are not used to reduce the approach speed, the shortest landing distance is obtained essentially at a power-off condition with a high rate of descent (about 1400 fpm). It was pointed out in reference 5 that landings made with low power were marginal because of the pilot's inability to accurately control flight path. Thus it is possible that the use of power can greatly reduce landing distance as well as provide more accurate control of the landing.

Stall margin.- The next table gives the speed increment above the stall speed for the same configurations as in the previous table:

				Conventional approach		STOL approach	
BLC	δ_f, deg	δ_a, deg	V_s, power on, k (1)	$1.3V_s$, power off, k	Stall margin, k	$1.15V_s$, power on, k (1)	Stall margin, k
off	40	0	75	112	37	86	11
on	80	30	50	87	37	58	8

[1]Power required for 500 fpm rate of descent.

For a STOL approach, the stall speed is dependent on thrust, and the loss of an engine, without corrective measures, will reduce the stall margin to about 5 knots. Reference 5 indicated that the stall margin should be no less than 10 knots, regardless of the ratio of approach to stall speed. To satisfy this requirement it would be necessary to increase the ratio of approach to stall speed over the value assumed for the present analysis, to increase $C_{L_{max}}$, or to provide interconnecting shafting. The effect of the loss of an engine on directional and lateral control will be discussed in a later section.

A 4 2 3

Figure 6 shows the effect of forward speed on the ratio of thrust to weight required at a 500 fpm rate of descent for an airplane with a wing loading of 50 psf. It may be noted that approaches made at 1.3 times the power-off stall speed are on the so-called stable side, whereas approaches at 1.15 times the power-on stall speed may be on the unstable side (also referred to as area of reverse command or back side of the thrust-velocity curve). It was pointed out in references 5 and 8 that no great difficulty was encountered in flying on the unstable side; however, since glide path was controlled primarily by varying power, a rapid and positive thrust response was required. To arrest the sink rate to make a "go around," installed thrust-to-weight ratios of at least 0.3 will be required. It is apparent that the thrust-to-weight ratio required for STOL landings with highly effective flaps can become sufficiently large to be a design consideration.

Take-off.- Take-off calculations were made to determine the effects of flap deflection, BLC, static thrust-to-weight ratio, wing loading, and take-off technique. These calculations were made to indicate trends, not to provide absolute values. The change of thrust with speed used for the calculations is shown in figure 7, and the appendix gives the method and assumptions used for the calculations. The results of some of these calculations are given in figures 8, 9, and 10 and in the table below. The take-off at 1.15 times the power-off stall speed would represent a conventional type of take-off (ref. 7); whereas the take-off at 1.15 times the power-on stall speed represents a maximum effort STOL take-off where slipstream effects have been used to reduce the take-off speed.[2]

---

[2]The calculations for the conventional take-off were made using a ground resistance of 0.03 representing concrete; whereas, those for the STOL take-off were made using a value of 0.1 representing hard sod.

$\frac{W}{S}$ = 50 lb/ft^2, $\frac{T_o}{W}$ = 0.3

BLC	δ_f, deg	δ_a, deg	Conventional take-off at 1.15V_s, power off		STOL take-off at 1.15V_s, power on	
			Take-off velocity, k	Total distance to 50 ft, ft	Take-off velocity, k	Total distance to 50 ft, ft
off	20	0	107	5800	80	2400
on	40	30	83	4000	62	2600
$\frac{W}{S}$ = 50 lb/ft^2, $\frac{T_o}{W}$ = 0.6						
off	20	0	107	2400	62	1000
on	40	30	83	1500	51	800

The calculations indicated that utilizing the slipstream effects to reduce the take-off speed greatly decreased the take-off distance to clear a 50-foot obstacle. Comparison of the distances obtained for the STOL take-off showed that BLC (on a higher flap deflection) did not reduce the take-off distances in all cases. This occurred because the increased lift obtained with the more effective flap was accompanied by increased induced drag which reduced the longitudinal acceleration and angle of climb.

The calculations previously presented did not consider the loss of an engine, which can reduce the stall margin, increase the take-off distance, and create a lateral and directional control problem. For the STOL cases presented in the previous table, the loss of an engine reduced the ratio of take-off to stall speed from 1.15 to about 1.05. As was discussed in the previous section, these ratios may be insufficient to provide an adequate margin in stall speed. To perform a conventional take-off with safety, the take-off field length is prescribed, in reference 7, as one where allowance is made for an engine failure so that the airplane can stop or continue and take-off on the remaining engines. The effect of this consideration on take-off speed and total take-off distance to 50 feet is presented in the following table. For the STOL case the take-off speed was taken as the value obtained for a thrust-to-weight ratio corresponding to 3/4 power. For convenience, it was assumed that no asymmetry in lift existed, thus representing the conditions obtained with interconnected propellers.

$\frac{W}{S}$ = 50 lb/ft^2, $\frac{T_o}{W}$ = 0.6

			Conventional take-off at 1.15V_s, power off		STOL take-off at 1.15V_s, power on	
BLC	δ_f, deg	δ_a, deg	Take-off velocity, k	Total distance to 50 ft, ft	Take-off velocity, k	Total distance to 50 ft, ft
off	20	0	107	2600	68	1300
on	40	30	83	1700	55	1000

A 4 2 3

Comparison of these values with those presented in an earlier table shows that for an installed thrust-to-weight ratio of 0.6 the take-off distance was increased about 200 feet by the loss of an engine. The effect of asymmetry on the minimum control speed will be considered in a later section.

From the foregoing discussion on landing and take-off performance, it is concluded that a highly effective flap in conjuction with a STOL technique can more than halve the landing and take-off distances. Further reductions in distance would be made possible by the use of a leading-edge device since reference 3 indicated that the $C_{L_{max}}$ was limited by airflow separation from the leading edge of the wing. The extent to which all these benefits can be utilized in practice will necessitate further flight experience to define the speed margin necessary for safety; this margin is influenced by severity of stall, type of operation, as well as the possibility of engine failure.

Longitudinal Stability and Control

The previous sections have shown the improvements in landing and take-off performance that can be obtained by the use of highly effective trailing-edge flaps combined with high thrust coefficients. In the following sections, the effects of these parameters on the stability and control characteristics will be discussed.

Longitudinal stability.- Representative pitching-moment characteristics of the four-propeller model reported in reference 4 are presented in figure 11. Data are shown for various values of thrust coefficient for flaps undeflected and deflected 60° with BLC. Tail-on and tail-off data are given for the center of gravity located horizontally at 0.25$\bar{c}$ and vertically at two positions: on the thrust axis and 0.35$\bar{c}$ below the thrust axis. These data were used to obtain the variations with speed of the attitude-stability derivative, C_{m_α}, and the speed-stability derivative, C_{m_V}, shown in figures 12 and 13, respectively. The reduction in C_{m_α} (tail on) with reduced forward speed resulted from the increase in the change of downwash angle with angle of attack, $d\epsilon/d\alpha$, as thrust

coefficient was increased at the lower speeds. Reference 4 showed[3] that $d\epsilon/d\alpha$ increased from a power-off value of 0.5 to a value of 1.0 at a thrust coefficient of 2.

Values of $\partial\epsilon/\partial\alpha$ would be lower and hence attitude stability (C_{m_α}) would be increased if the horizontal tail were located higher relative to the wing. Lowering the center of gravity has a beneficial effect on C_{m_α} because of the relative displacement between the center of gravity and the wing aerodynamic center as angle of attack is increased. The horizontal location of the center of gravity for $C_{m_\alpha} = 0$, the neutral point, is shown in figure 14.

The static stability derivatives and estimated damping characteristics were used to determine the dynamic characteristics of the assumed airplane at the low speeds. The adequacy of these characteristics was evaluated on the basis of the criteria set forth in reference 6. The calculated dynamic characteristics for the short-period mode are given in figure 15. The only requirement for this mode given in reference 6 for the landing configuration is that the damping ratio be greater than 0.055 for periods less than 5 seconds. Since the calculated motion of the assumed airplane is "deadbeat" (damping ratio greater than 1, fig. 15), this requirement is satisfied. However, reference 9 indicates that for the combination of damping ratio and natural frequency shown in figure 15, the airplane response would be rather sluggish. The calculated dynamic characteristics for the long-period mode (phugoid) are given in figure 16. Since positive damping exists throughout the speed range and since the period is greater than 10 seconds, no problem would be anticipated with the phugoid motion for the assumed airplane. However, figure 16 indicates that the airplane may be dynamically unstable at lower speeds where values of C_{m_V} are high.

Longitudinal control.- Associated with STOL performance are longitudinal control problems that can result from stalling of the horizontal tail, and a reduction in pitching moment available from the stabilizer and elevator due to the low free-stream dynamic pressure. Typical variations of pitching-moment coefficient with lift coefficient are shown in figure 17 for several stabilizer and elevator configurations for the model with flaps deflected 80° and BLC applied. Figure 17(a) shows the effect of air-flow separation on the horizontal tail which resulted from the large downwash angle produced by the large flap deflection and thrust coefficient used. This stalling must be avoided if satisfactory longitudinal control is to be retained throughout the operating range. If the out-of-trim pitching moments are not too large, the tail stall can be avoided by using a horizontal tail with adjustable incidence (fig. 17(a)); however, it may be desirable to add a leading-edge flap with BLC (fig. 17(b)). With no stall on the leading edge of the tail, longitudinal control can be increased by

[3]Unpublished data obtained with a survey rake showed that the dynamic pressure at the tail was approximately that of the free stream throughout the range of angles of attack, flap deflections, and thrust coefficients tested.

increasing elevator deflection and applying BLC to the elevator (fig. 17(c)). The effects of elevator deflection, nose flap, and BLC on the horizontal-tail lift coefficient calculated from the pitching-moment coefficients are summarized in figure 18.

The elevator deflection required to balance the pitching moment and maintain level unaccelerated flight is shown in figure 19(a) for the airplane with the horizontal center of gravity at $0.25\bar{c}$. This figure shows that sufficient control is available to develop $C_{L_{max}}$ as specified in reference 6. Figure 19(b) gives the pitching acceleration possible (after the airplane is trimmed) with a conventional fixed tail and with an adjustable-incidence tail plus BLC on the elevator. These values are compared with the requirement for hovering (ref. 6). Based on these calculations, the assumed airplane would have adequate longitudinal control throughout the STOL speed range. In addition, when BLC is applied to the elevator some control is available to cope with center-of-gravity movements.

Lateral and Directional Characteristics

Figure 20 presents the variations of yawing-moment, rolling-moment and side-force coefficients with sideslip angle for the complete four-propeller model for several thrust coefficients at zero angle of attack with flaps and ailerons either undeflected or deflected with BLC applied. Data at other angles of attack show trends similar to those presented. The lateral and directional stability derivatives for this model with numerous flap configurations are summarized in figure 21. These data represent average values over a small sideslip range through zero sideslip angle and at zero angle of attack.

Directional stability and dihedral effect.- With the flaps deflected and at high T_c', the variation of C_n with β is reversed at positive β's (fig. 20). This characteristic is unacceptable (ref. 6). The low dihedral effect is unsatisfactory, and when coupled with a moderate value for the directional stability parameter, C_{n_β}, generally results in a spiral divergence type of instability. An analysis of the dynamic lateral motions was not made; however, the data do show that the large flap deflections and high thrust required to improve landing and take-off performance may have a detrimental effect on lateral and directional stability characteristics.

Side force.- The data of figure 22 show that a large side force occurs as angle of attack and thrust coefficients are increased. This results from the use of propellers with the same rotation. The data also show that the side forces are considerably larger with the four-propeller model than with the two-propeller model. The data presented indicate that the side force was not due to flow-field changes at the tail surfaces. Additional data not presented indicated that the side force did not result

from flow separation on the wing, and that the side force was eliminated by the use of counterrotating propellers. It is conjectured that the side force measured with rotating propellers was due to the flow field in which the propellers were operating when the model was at high lift. This flow field (combined angle of attack, upwash, and vertical velocity gradients) can cause in-plane propeller forces as well as change the flow around the fuselage. The reason the side forces were larger with the four-propeller model than with the two-propeller model is not known; however, the propeller advance ratios for equal T_c' were substantially different. To balance the side force by sideslipping and holding the wings level would require large rudder and aileron deflections. Lower control deflections would be required if the airplane were banked to a moderate angle (of the order of 5° at the maximum lift) so that the side force would be balanced by a component of the airplane weight. This side-force problem can be avoided by using counterrotating propellers.

A 4 2 3

Lateral control, symmetric power.- Pilot opinion of aircraft roll performance was shown in references 10 and 11 to be related to damping, inertia, and control power. Reference 11 pointed out that angular displacement in a given time rather than initial acceleration is a quantity more directly appreciated by the pilot in correcting attitude deviations. However, it should be recognized that angular displacement and initial acceleration are related by the damping. This relationship is given in reference 6 along with tentative criteria based on gross weight (the lower limit, regardless of gross weight is 15° at end of 1 second). This reference also specified a minimum value of damping. These criteria for the hypothetical airplane being considered are shown in figure 23 where initial rolling acceleration is plotted against the roll time constant.[4] Included for comparative purposes in figure 23 are the values of initial acceleration calculated from the measured rolling moment obtained with and without BLC applied to the ailerons (ref. 3). The time constant is based on a constant damping value, C_{l_p}, obtained from reference 12.

It can be seen that the requirement of 15° at the end of 1 second is the more difficult one to meet because of the large weight of the airplane. This requirement can be met with ailerons without BLC only at speed above approximately 110 knots; whereas addition of BLC to the ailerons reduced this speed to 65 knots. The data of figure 23 indicate that sufficient damping would be obtained throughout the landing and take-off speed range. Increased lateral control at lower speeds may be obtained by supplementing the ailerons with differentially deflected flaps, by immersing the ailerons in the slipstream, by the addition of spoilers, or by the use of differential propeller pitch.

Lateral and directional control with asymmetric power.- The minimum control speed of a multiengine airplane is usually limited by the directional control power available to maintain a heading in a take-off configuration with one engine inoperative and the remaining engines developing

[4]This constant is the time required for the angular velocity to reach 63 percent of the steady value following a control input.

take-off power (ref. 7). On STOL vehicles an inoperative engine can also cause large rolling moments due to the loss in lift on the one side. In addition, the landing speeds can be as low or lower than take-off speeds, and take-off power may be required to arrest the sink and effect a "go around." For these reasons it is desirable to examine the minimum control speed in the landing as well as the take-off configuration.

The change in yawing- and rolling-moment coefficients measured with the left outboard engine inoperative on the four-propellered model are presented in figure 24, for two flap configurations with several thrust conditions based on thrust values prior to asymmetry. Also included in these figures are the rudder and aileron deflections required to maintain zero sideslip with the wings level. These deflections are based on rudder and aileron control power with BLC applied to each. Based on these data, it appears that the airplane can be controlled with zero sideslip down to a speed of about 60 knots, the speed range for the STOL landings and take-offs of the assumed airplane. Without BLC on these control surfaces, the corresponding minimum control speed would be considerably higher. The minimum control speed can be reduced by allowing the airplane to sideslip and bank to the maximum value of 5° specified in reference 6. Interconnecting the propellers would eliminate the minimum control speed as presently defined; however, failure of the propeller pitch mechanism could then impose a control limit.

A 4 2 3

BLC Pump Considerations

The previous discussion has been based on the aerodynamic characteristics obtained with blowing type of BLC. The following discussion will briefly compare the lift characteristics of different BLC systems. In addition, an assessment of the power and weight penalties of these systems will be made. The lift obtained and flow required with area suction and moderately high-pressure blowing forms of BLC are summarized in figures 25 and 26. These data were measured with the two-propellered model reported in references 2 and 3. It would be expected that similar comparative results would be obtained with the four-propellered model.

Larger lift increments are obtained with blowing than with area suction for several reasons. Blowing will maintain more complete flow attachment; this is evidenced in figure 25 by the larger lift increment (power off) for equal flap deflections. In addition, increasing the flap deflection beyond 60° did not increase the lift provided by area suction, but did increase the lift obtained with blowing. The values of lift shown in figure 25 are for flow and momentum coefficients near the lowest values required to maintain attached flow on the flap. Increasing the flow coefficients beyond these values produced no increase in lift with area suction; whereas increases in lift were obtained with blowing. It is interesting to note that the difference between the lift obtained with suction and blowing, at 60° of flap deflection, decreases as the thrust

coefficient is increased. The flap lift increments for the combination slot suction and low-pressure blowing system (Arado system of ref. 1) appear to lie between those shown for suction and for blowing. In general, flight and wind-tunnel results have shown that the anticipated increments are usually more difficult to obtain with an area suction system than with blowing. Area suction is more sensitive to upsetting disturbances resulting from discontinuities due to cutouts for flap mechanisms and slats, or from the rough flow caused by fuselage boundary layer.

Examples of pumping powers and estimated pumping system weights are tabulated below for the assumed airplane with a 50-pound-per-square-foot wing loading making a landing approach with a descent rate of 500 ft/min.

	Conventional approach			STOL approach		
	$1.3V_s$, power off, k	Adiabatic hp	$\frac{W_{pump}}{W_{airplane}}$	$1.15V_s$, power on, k	Adiabatic hp	$\frac{W_{pump}}{W_{airplane}}$
Blowing, $\delta_f = 80^\circ$ $C_{\mu_f} = 0.050$ $h_j/\bar{c} = 0.00088$	87	2040	0.033	53	680	0.011
Blowing, $\delta_f = 60^\circ$ $C_{\mu_f} = 0.035$ $h_j/\bar{c} = 0.00088$	91	1730	0.028	67	766	0.012
Area suction, $\delta_f = 60^\circ$ $C_{Q_f} = 0.0015$	96	185	0.003	70	86	0.001

For these calculations, it was assumed that sufficient pumping capacity was provided to give the desired flow coefficient at the approach speed. The approach was made with a 30° drooped aileron and sufficient capacity was provided for 60° of aileron deflection. The corresponding flow coefficient requirements for both ailerons are $C_{\mu_a} = 0.018$ with blowing and $C_{Q_a} = 0.0008$ with area suction. It was assumed that duct losses were small. Based on existing self-contained gas turbine compressors, a value of 1.0 was used for the ratio, adiabatic hp/W_{pump}. For the blowing system, the power required would depend on the nozzle height chosen. Increasing the nozzle height decreases the air horsepower; however, the resulting increase in flow quantity could increase the duct losses sufficiently to overbalance the reduction in air horsepower. Only a detailed analysis of the specific design of the complete BLC system would provide sufficient information to choose the optimum nozzle height for a particular airplane.

CONCLUDING REMARKS

A study of the take-off and landing distances possible with a conventional propeller-driven transport-type airplane indicated that if highly effective flaps were used in combination with large amounts of power to augment lift (STOL), the landing and take-off distances would be less than half of the distances for conventional operation. The study is based on the wind-tunnel tests of a model with BLC on the trailing-edge flaps and control surfaces. At the lowest speeds considered (about 50 knots), adequate longitudinal stability was obtained but the lateral and directional stability were unsatisfactory. At these low speeds the conventional aerodynamic control surfaces may not be able to cope with the forces and moments produced by symmetric as well as asymmetric engine power. This problem was alleviated by increasing control effectiveness by use of BLC. Further reductions in the landing and take-off speeds to obtain shorter distances probably will result in the need to supplement the aerodynamic controls, the need for counterrotating propellers, and possibly the need for interconnected shafting on the propellers.

Ames Research Center
National Aeronautics and Space Administration
Moffett Field, Calif., April 18, 1961

REFERENCES

1. Fink, Marvin P., Cocke, Bennie W., and Lipson, Stanley: A Wind-Tunnel Investigation of a 0.4-Scale Model of an Assault Transport Airplane With Boundary-Layer Control Applied. NACA RM L55G26a, 1956.

2. Weiberg, James A., Griffin, Roy N., Jr., and Florman, George, L.: Large-Scale Wind-Tunnel Tests of an Airplane Model With an Unswept, Aspect-Ratio-10 Wing, Two Propellers, and Area-Suction Flaps. NACA TN 4365, 1958.

3. Griffin, Roy N., Jr., Holzhauser, Curt A., and Weiberg, James A.: Large-Scale Wind-Tunnel Tests of an Airplane Model With an Unswept, Aspect-Ratio-10 Wing, Two Propellers, and Blowing Flaps. NASA MEMO 12-3-58A, 1958.

4. Weiberg, James A., and Page, V. Robert.: Large-Scale Wind-Tunnel Tests of an Airplane Model With an Unswept, Aspect-Ratio-10 Wing, Four Propellers, and Blowing Flaps. NASA TN D-25, 1959.

5. Innis, Robert C., and Quigley, Hervey C.: A Flight Examination of the Operating Problems of V/STOL Aircraft in STOL-Type Landing and Approach. NASA TN D-862, 1961.

6. Anderson, Seth B.: An Examination of Handling Qualitites Criteria for V/STOL Aircraft. NASA TN D-331, 1960.

7. Anon.: Airplane Airworthiness, Transport Categories Civil Aeronautics Manual 4b. Department of Commerce, Sept. 1954.

8. Drinkwater, Fred J., III, and Cooper, George E.: A Flight Evaluation of the Factors Which Influence the Selection of Landing Approach Speeds. NASA MEMO 10-6-58A, 1958.

9. Chalk, Charles R.: Additional Flight Evaluations of Various Longitudinal Handling Qualities in a Variable-Stability Jet Fighter. WADC Tech. Rep. 57-719, pt. I, ASTIA Document No. 142184, 1958.

10. Creer, Brent Y., Stewart, John D., Merrick, Robert B., and Drinkwater, Fred J., III.: A Pilot Opinion Study of Lateral Control Requirements for Fighter-Type Aircraft. NASA MEMO 1-29-59A, 1959.

11. Tapscott, R. J.: Criteria for Control and Response Characteristics in Hovering and Low Speed Flight. Aero/Space Engineering, June 1960, pp. 38-41.

12. DeYoung, John: Theoretical Antisymmetric Span Loading for Wings of Arbitrary Plan Forms at Subsonic Speeds. NACA Rep. 1056, 1951.

13. Kettle, D. J.: Ground Performance at Take-Off and Landing. Aircraft Engineering, vol. XXX, no. 347, Jan. 1958, p. 2.

14. Lovell, J. Calvin, and Lipson, Stanley: An Analysis of the Effect of Lift-Drag Ratio and Stalling-Speed on Landing-Flare Characteristics. NACA TN 1930, 1949.

APPENDIX

EQUATIONS AND ASSUMPTIONS USED FOR LANDING AND TAKE-OFF CALCULATIONS

LANDING

Air Distance

A 4 2 3

The air distance consists of the approach distance in the steady glide plus the flare distance $s_a + s_f$. If a circular arc and small angle are assumed,

$$s_a = \frac{50}{\tan \gamma} - \frac{s_f}{2}, \text{ ft}$$

$$s_f = \frac{2V^2}{g\ \Delta n} \tan \frac{\gamma}{2} = \frac{V^2}{g\ \Delta n}\ \gamma, \text{ ft}$$

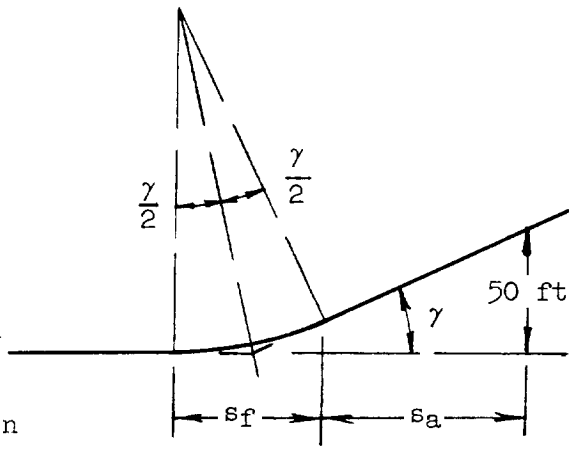

where

V velocity during the flare; assumed equal to the approach speed in feet per second

Δn increment of normal acceleration developed in the flare (a value of 0.1 was used)

γ glide angle

Ground Roll, s_g

$$s_g = \frac{30\ \frac{W}{S}}{-\sigma\left(C_{D_G} - \mu C_{L_G}\right)} \log_{10} \frac{\mu - \frac{T}{W}}{\mu - \frac{T}{W} + \frac{C_{D_G} - \mu C_{L_G}}{C_{L_{TD}}}}, \text{ ft} \qquad \text{reference 13}$$

where

σ ratio of air density to standard value; $\sigma = 1$ was used

μ braking coefficient; $\mu = 0.35$ was used

$\frac{T}{W}$ thrust-to-weight ratio during ground roll; T/W = 0 was used

$C_{L_{TD}}$ lift coefficient at touchdown; a value equal to that for the approach was used

C_{L_G} lift coefficient during ground roll. A power-off value corresponding to $\alpha = -6^\circ$ was used except when a further reduction was required to reduce C_{L_G} to $C_{L_{TD}}$; for example, conventional approach with BLC on flaps

C_{D_G} drag coefficient during ground roll. A power-off value corresponding to the assumed ground-roll attitude was used

The calculations were made to indicate trends and not to provide absolute values. It is expected that more accurate values can be obtained by the use of reference 14 (also see ref. 5), which requires increasing excess speed margin to flare as the glide angle is steepened. Solution of the equations in reference 14 required iteration and only several examples were tried. The results indicated greater total landing distances, particularly at the steeper glide angles; consequently, a more shallow glide angle than was shown in figure 4 would be indicated for minimum landing distance.

TAKE-OFF

Ground Run, s_g

$$s_g = \int_{t=o}^{t=\text{take-off}} V\,dt \text{ , ft}$$

This equation was solved by graphical integration over the time of take-off, after the calculation of $\Delta t = \Delta V/a_{av}$ where the acceleration was calculated from $a = (g/W)[T-D-\mu(W-L)]$ at increments of 10 or 20 feet per second. The values of D and L were calculated from the wind-tunnel data at a fuselage angle of attack of -6° which corresponded to a wing angle of attack of about 0°. It was also assumed that rotation to lift off, when required, was initiated at a velocity 10 feet per second prior to the take-off velocity. A rolling resistance coefficient, μ, of 0.03 (corresponding to concrete) was used for the conventional take-off (made at 1.15 times the power-off stall speed); whereas a μ of 0.10 (corresponding to hard sod) was used for the STOL take-off (made at 1.15 times the power-on stall speed).

Transition and Climb to 50 Feet, s_t

Values were obtained by a step-by-step calculation and summation (at 0.1 second intervals) of the following equations:

$$V_{n+1} = V_n + \left(\frac{dV}{dt}\right)_n \Delta t$$

where

$$\left(\frac{dV}{dt}\right)_n = g\left(\frac{T}{W} - \frac{D'}{W} - \sin\gamma\right)$$

and

$$\gamma_{n+1} = \gamma_n + \left(\frac{d\gamma}{dt}\right)_n \Delta t$$

where

$$\left(\frac{d\gamma}{dt}\right)_n = \frac{g}{V}\left(\frac{L}{W} - \cos\gamma\right)$$

$$\Delta s = \Delta t V \cos\gamma \text{ , ft}$$

$$\Delta h = \Delta t V \sin\gamma \text{ , ft}$$

In these equations γ is the angle of climb, and the initial point $\gamma_{n=o}$ was taken as 0^o. The initial speed $V_{n=o}$ was 1.15 times the power-off or power-on stall speed, depending on the type of take-off. The succeeding speed in the transition was then dependent on the acceleration calculated. It was assumed that the transition was made at an angle of attack corresponding to the value required for lift off.

COMMENTS

Large variations in take-off, transition, and climb distances can be obtained by using different techniques and assumptions; no attempt was made to optimize take-off distance in the calculations made. When BLC was used, it was assumed that a constant flow coefficient was maintained throughout the speed range. For practical cases, this would generally not be true since the mass flow rather than flow coefficient would probably remain fairly constant; it would be expected that in such a case some increase in ground-roll distance may be incurred. Because of the use of high-lift flaps and/or high thrust-to-weight ratios, it was necessary to re-examine classical or so-called standard take-off, transition, and climb

equations. It was found necessary to discard take-off equations that assumed constant or average values of C_L and C_D, and transition and climb equations that either ignored transitior or required high normal acceleration to perform the maneuver.

TABLE I.- GENERAL GEOMETRIC DIMENSIONS OF THE MODEL

Dimension	Wing	Horizontal surface	Vertical surface
Area, sq ft	205.4	56.5	30.6
Span, ft	45.00	16.03	7.19
$\bar{c}$, ft	4.73	3.50	4.68
Aspect ratio	9.86	4.55	1.69
Taper ratio	0.50	0.45	0.55
Geometric twist, deg	4.8 (washout)	0	0
Dihedral from reference plane, deg	0.8	0	---
Incidence from reference plane, deg	8.3	---	---
Section profile (constant)	NACA 23017	NACA 0012	NACA 0012
Root chord, ft	6.07	4.61	5.88
Tip chord, ft	3.06	2.54	2.65
Sweep of leading edge, deg	2	12	24
Tail length, ft	---	18.01[a]	---

[a]Distance from $\bar{c}_w/4$ to $\bar{c}_t/4$.

TABLE II.- GEOMETRY OF AIRPLANE ASSUMED FOR STABILITY AND CONTROL CALCULATIONS

Wing	
Area, sq ft	1235
Span, ft	110
$\bar{c}$, ft	11.65
Horizontal surface	
Area, sq ft	340
Span, ft	39.2
$\bar{c}$, ft	8.56
Tail length, ft	44.4
Vertical surface	
Area, sq ft	182
Span, ft	17.6
$\bar{c}$, ft	11.45
Propeller diameter, ft	11.66
Gross weight, lb	61,800
Moment of inertia	
I_x, slug ft^3	355,000
I_y, slug ft^3	227,000
I_z, slug ft^3	522,000
Damping in roll, C_{l_p}	0.53

A
4
2
3

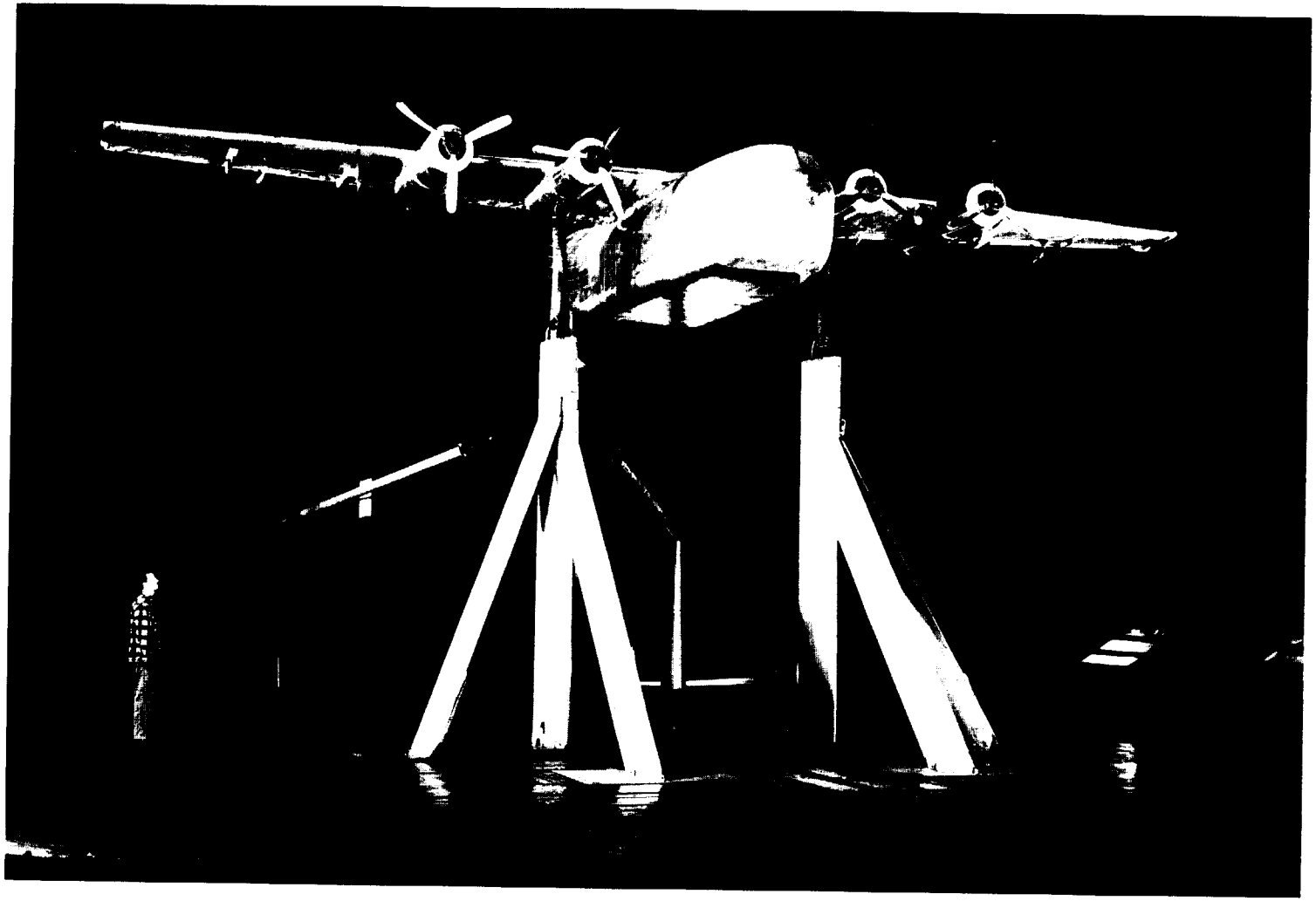

A-23743

(a) Photograph of model installed in the Ames 40- by 80-Foot Wind Tunnel.

Figure 1.- Model description.

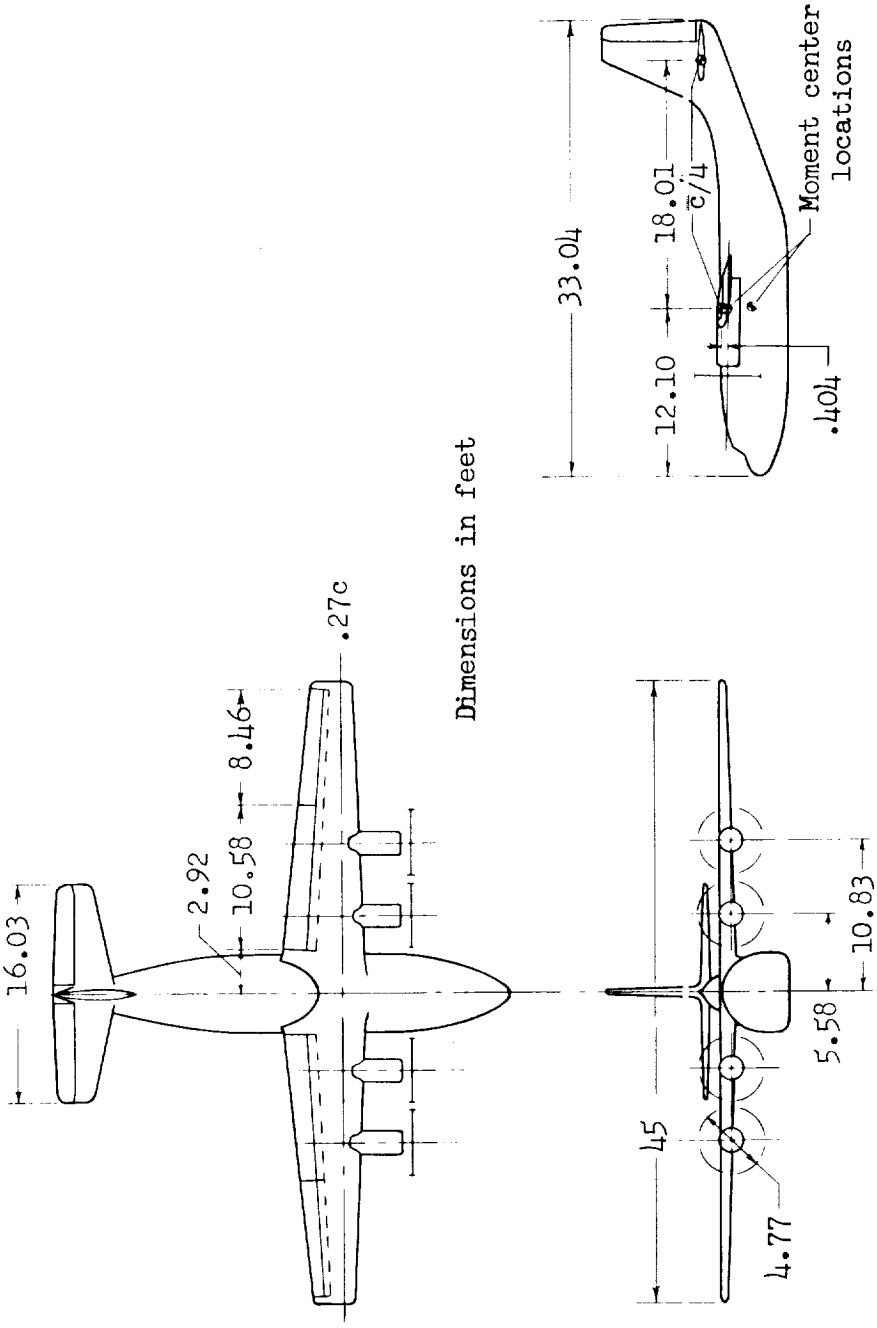

(b) Geometry of the model.

Figure 1.- Continued.

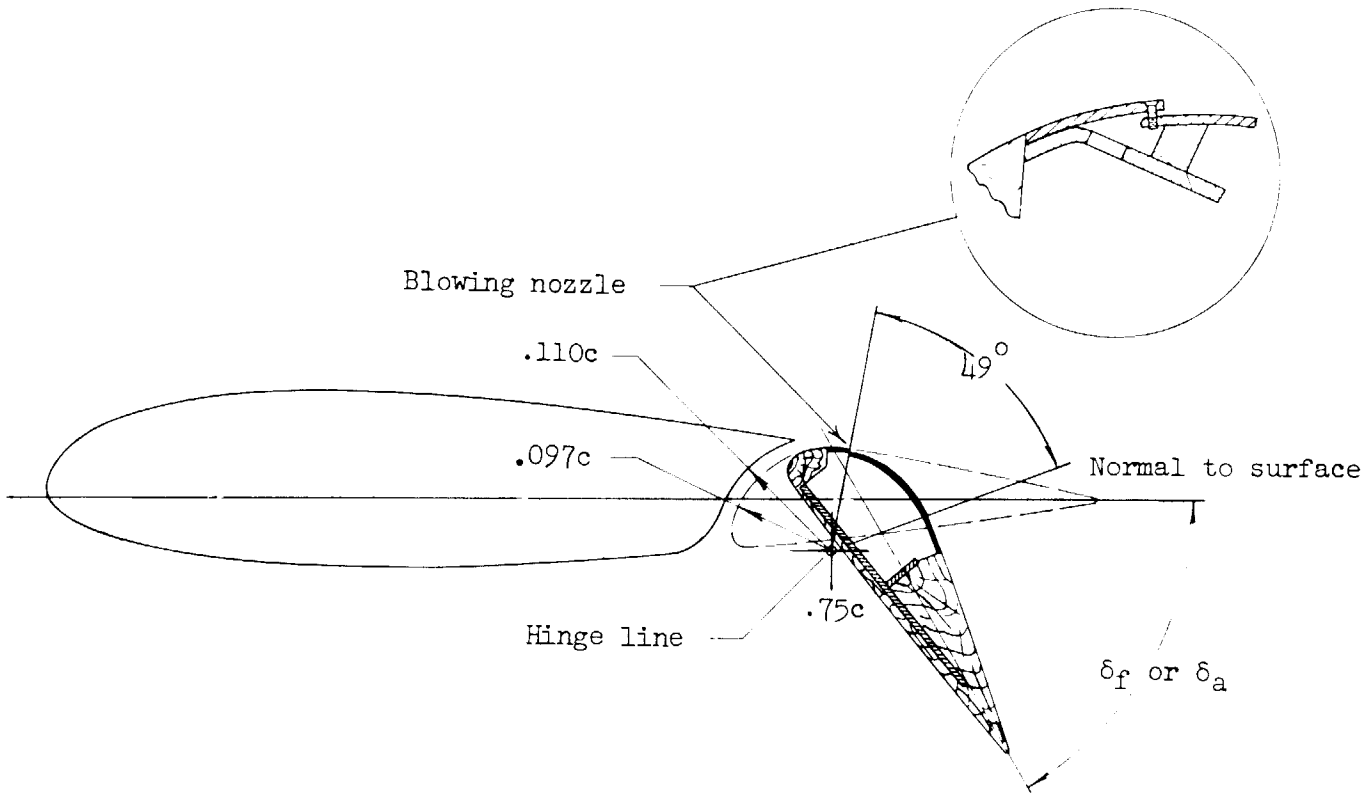

(c) Details of the flaps and ailerons.

Figure 1.- Continued.

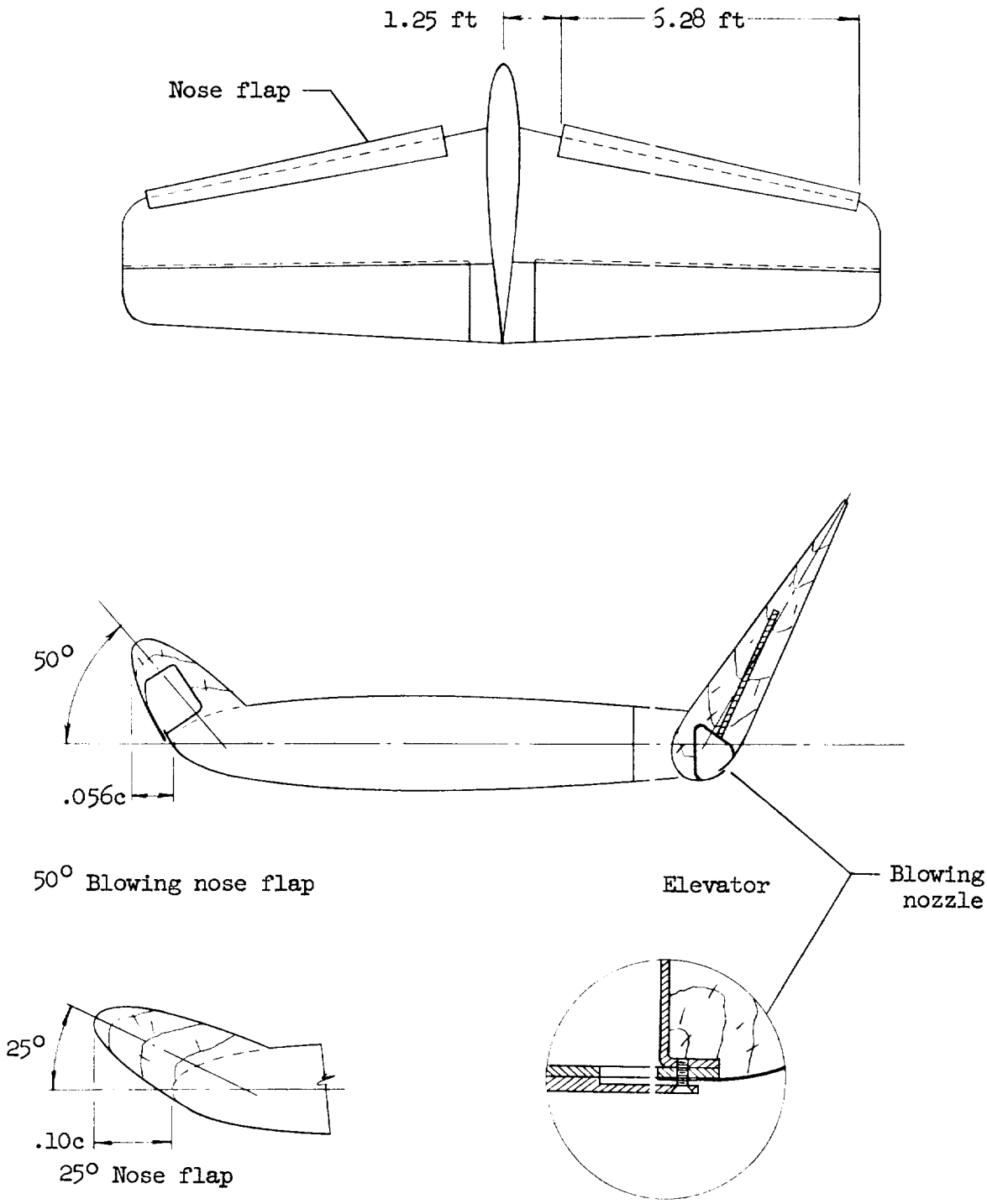

(d) Details of horizontal tail.

Figure 1.- Concluded.

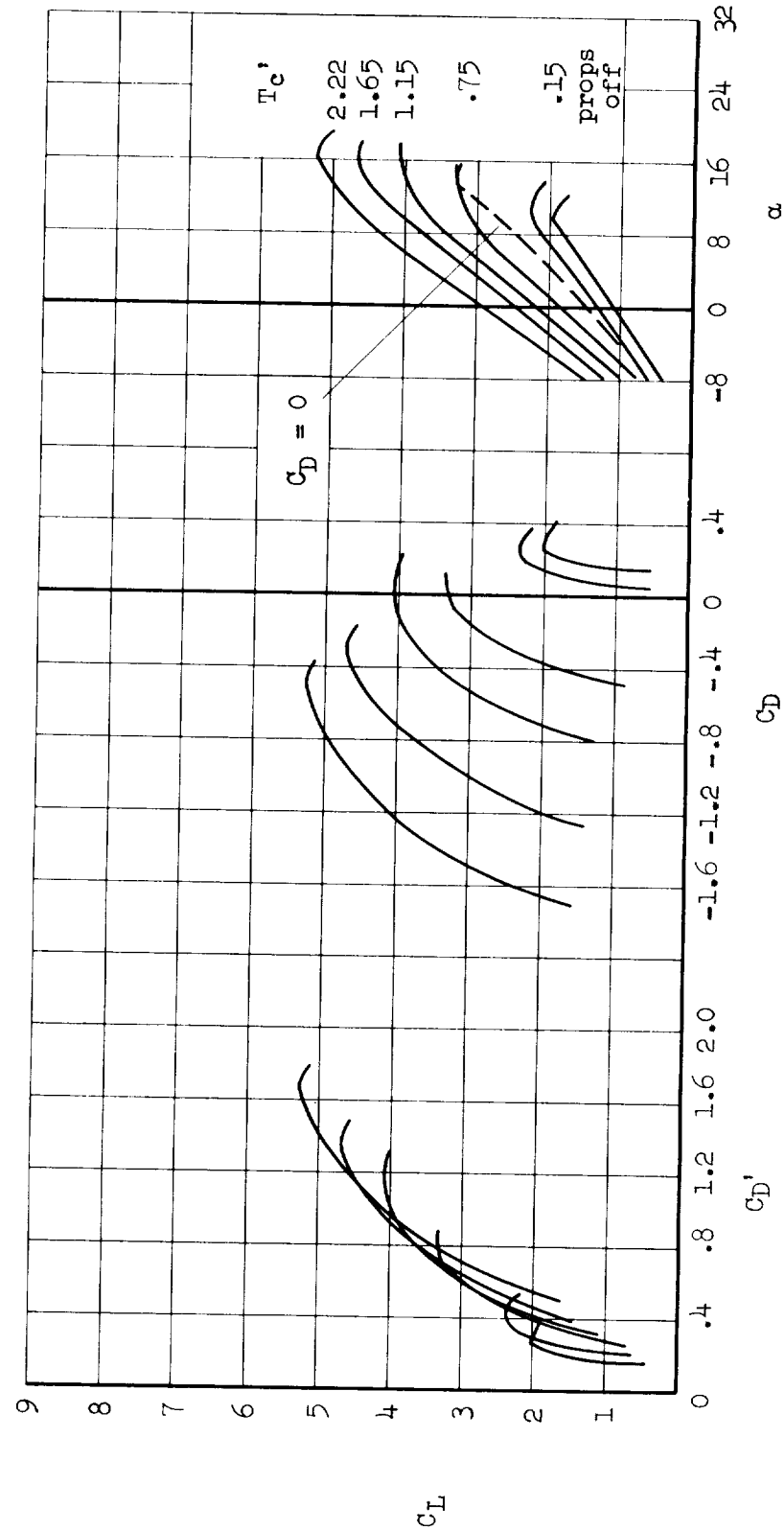

(a) $\delta_f = 40^\circ$; $\delta_a = 0^\circ$; no BLC.

Figure 2.- Lift and drag characteristics of the four-propeller model.

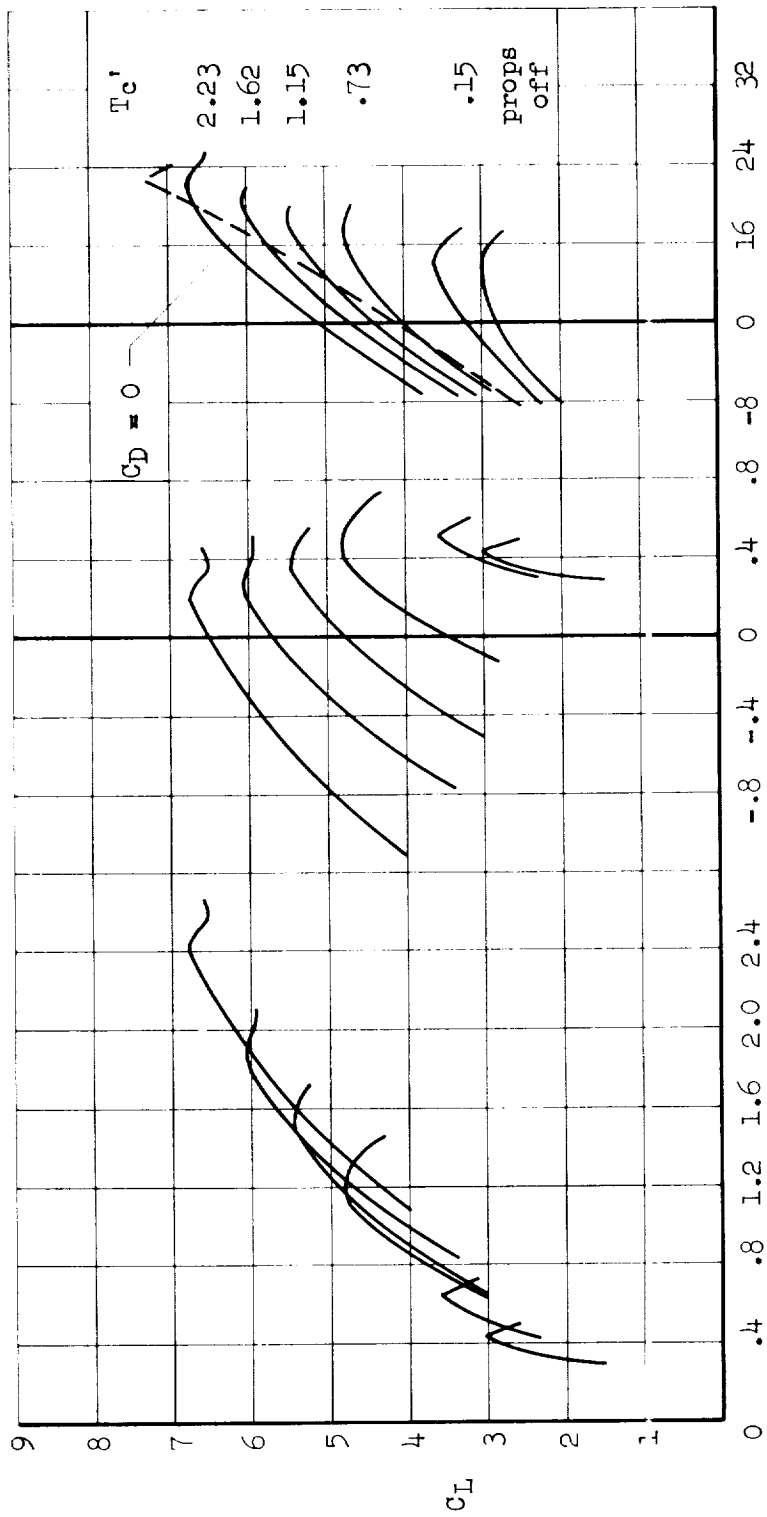

(b) $\delta_f = 60^\circ$, $\delta_a = 30^\circ$; BLC on both.

Figure 2.- Concluded.

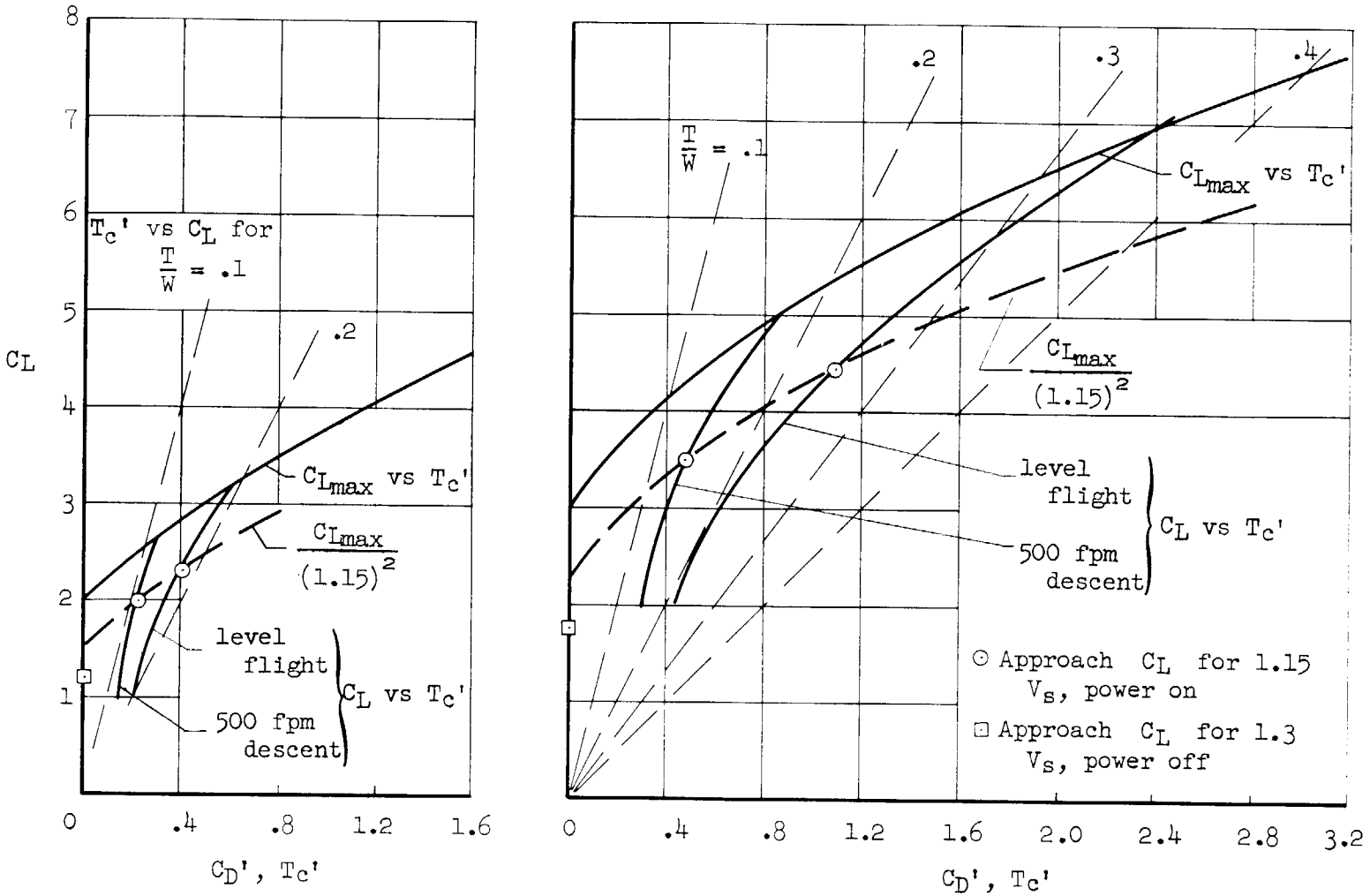

(a) $\delta_f = 40^\circ$, $\delta_a = 0^\circ$; no BLC

(b) $\delta_f = 60^\circ$, $\delta_a = 30^\circ$; with BLC.

Figure 3.- Approach lift coefficients for unaccelerated flight.

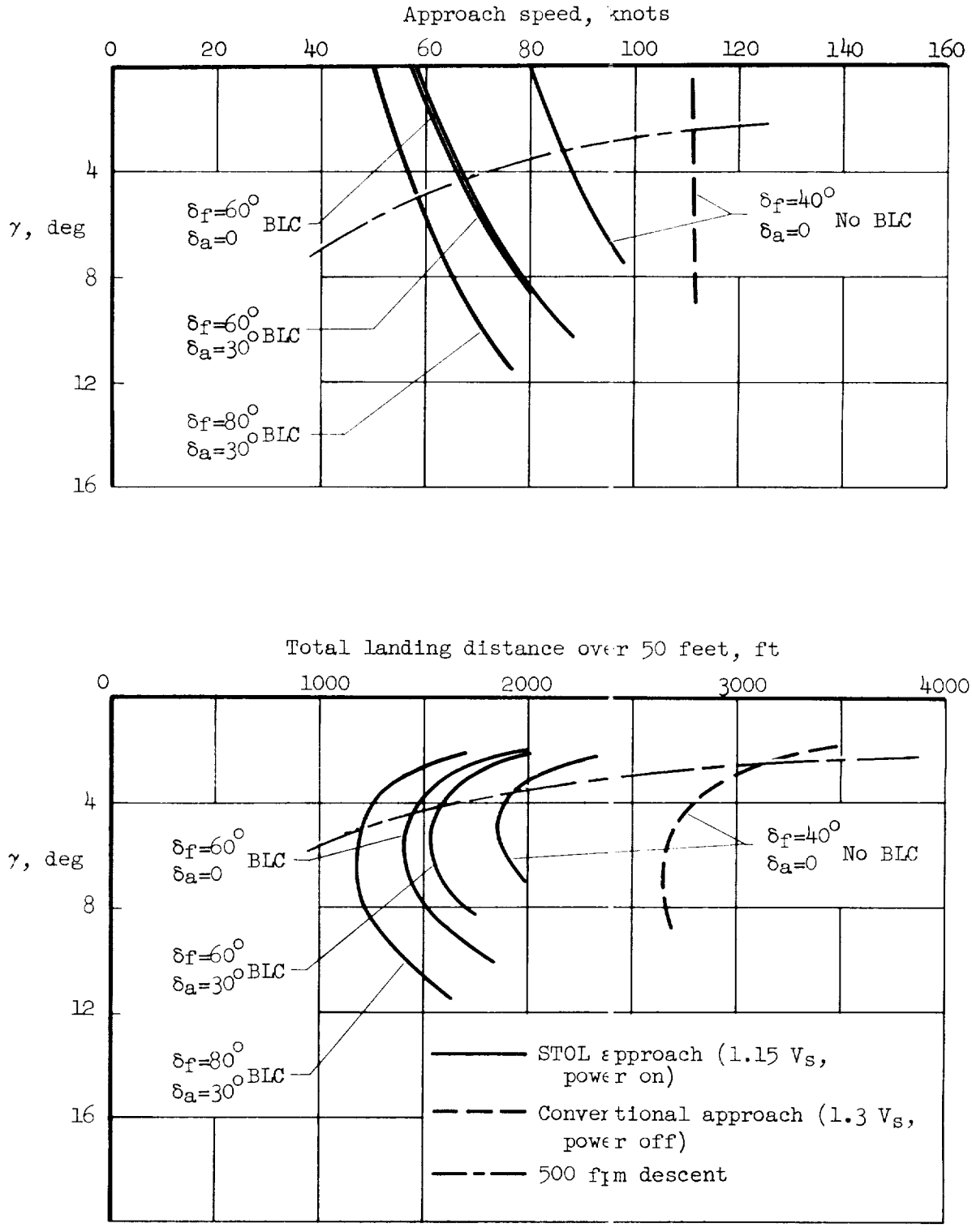

Figure 4.- Effect of glide angle on approach speed and landing distance over a 50-foot obstacle; W/S = 50 lb/ft^2, μ = 0.35.

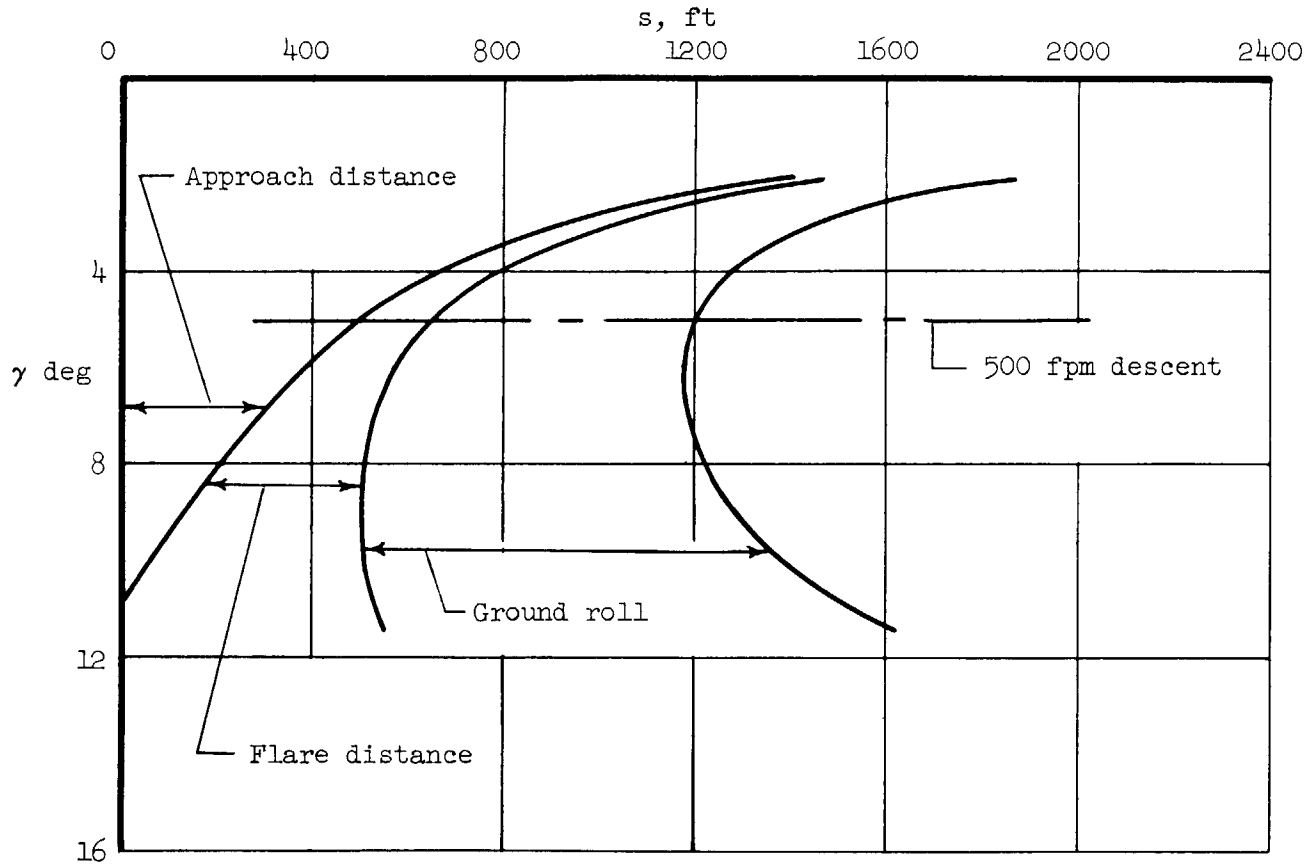

Figure 5.- Variation of air distance, flare distance, and ground roll with glide angle for STOL approach at 1.15 times the power-on stall speed; $\delta_f = 80^\circ$, $\delta_a = 30^\circ$, BLC on, $\mu = 0.35$, $W/S = 50$ lb/ft^2.

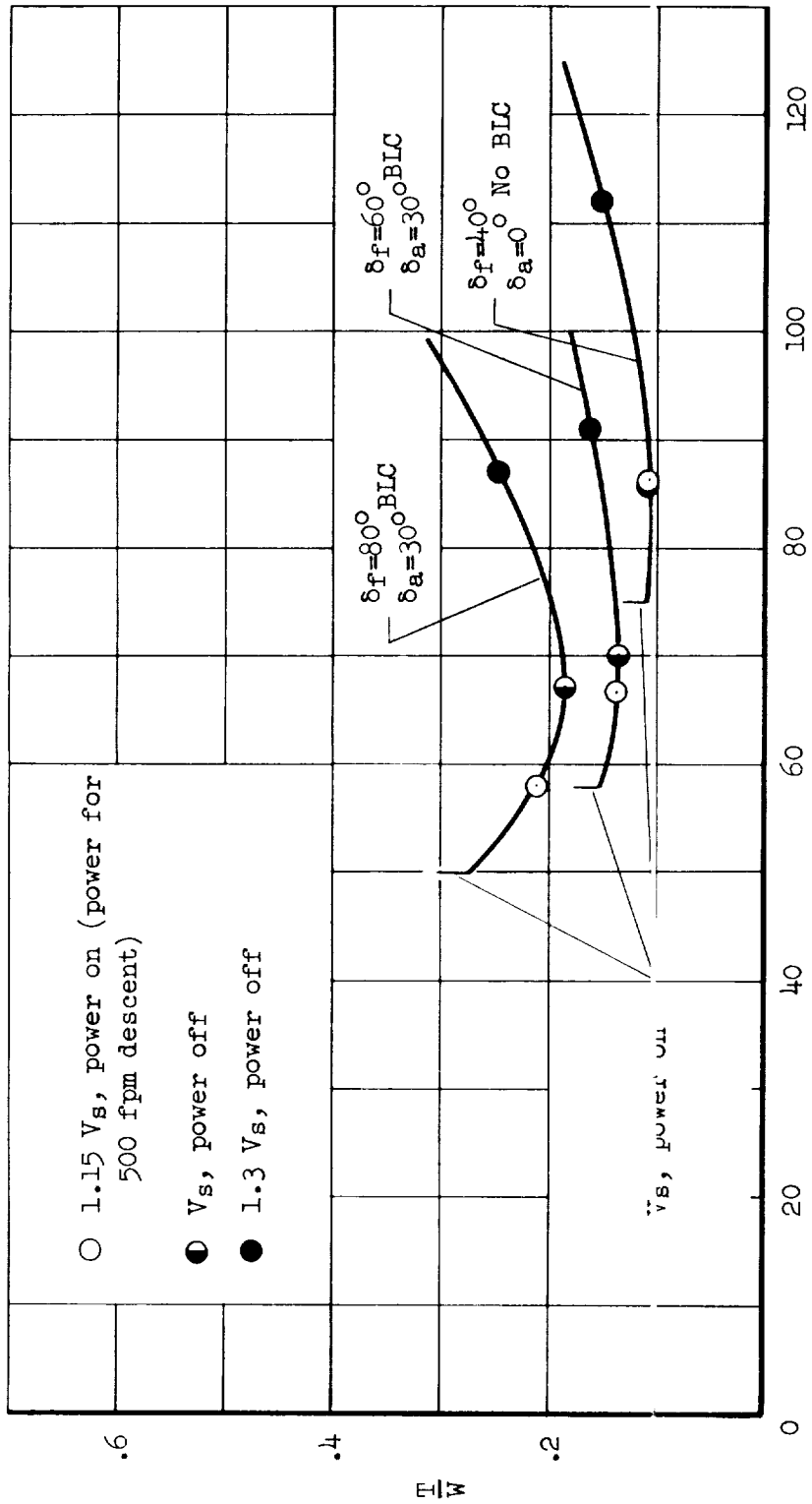

Figure 6.- Variation of thrust-to-weight ratio with speed for landing approach at 500-feet-per-minute rate of descent; W/S = 50 lb/ft^2.

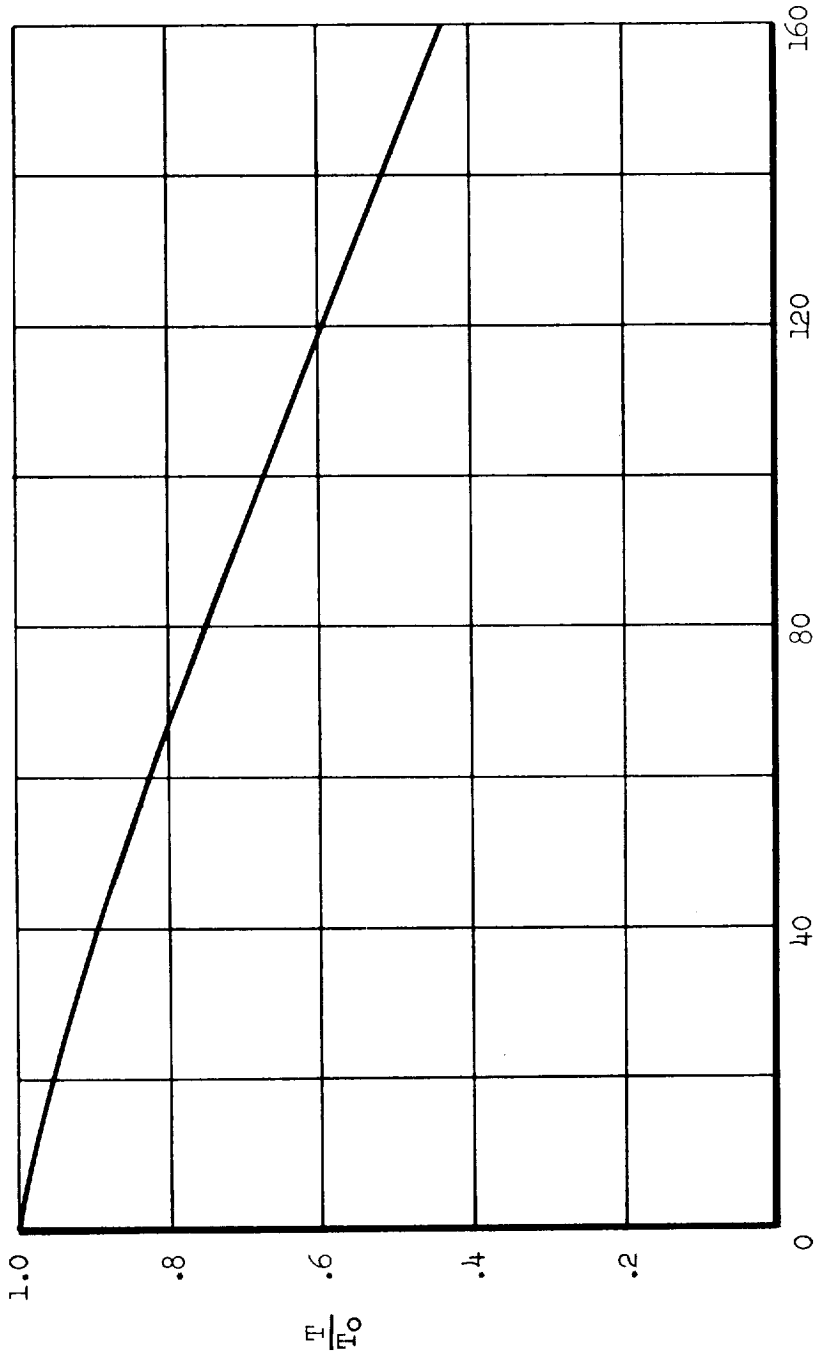

Figure 7.- Assumed thrust variation with velocity.

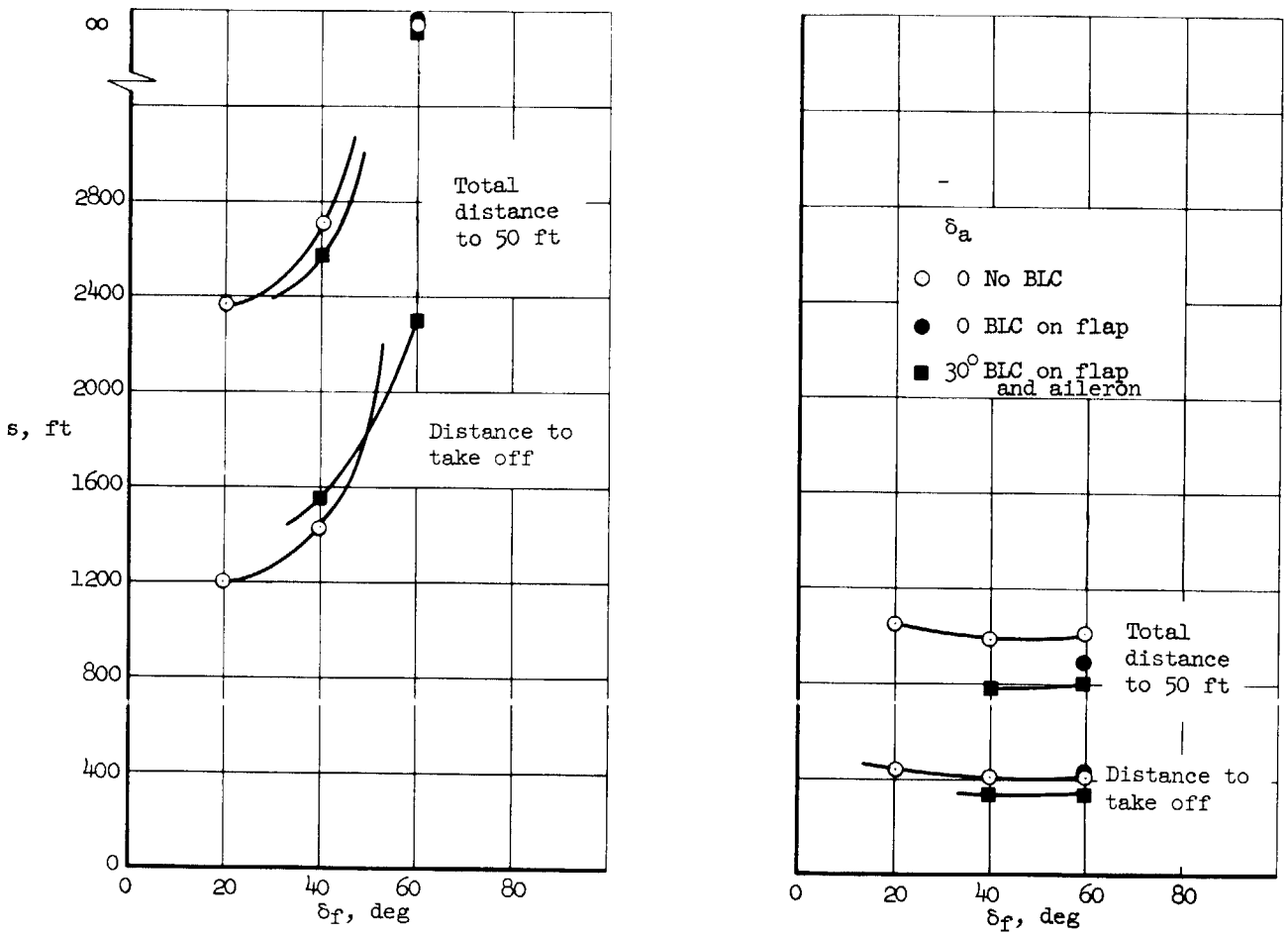

Figure 8.- STOL take-off as affected by flap deflection and BLC; take-off speed equal to 1.15 times the power-on stall speed; W/S = 50 lb/ft^2, μ = 0.1.

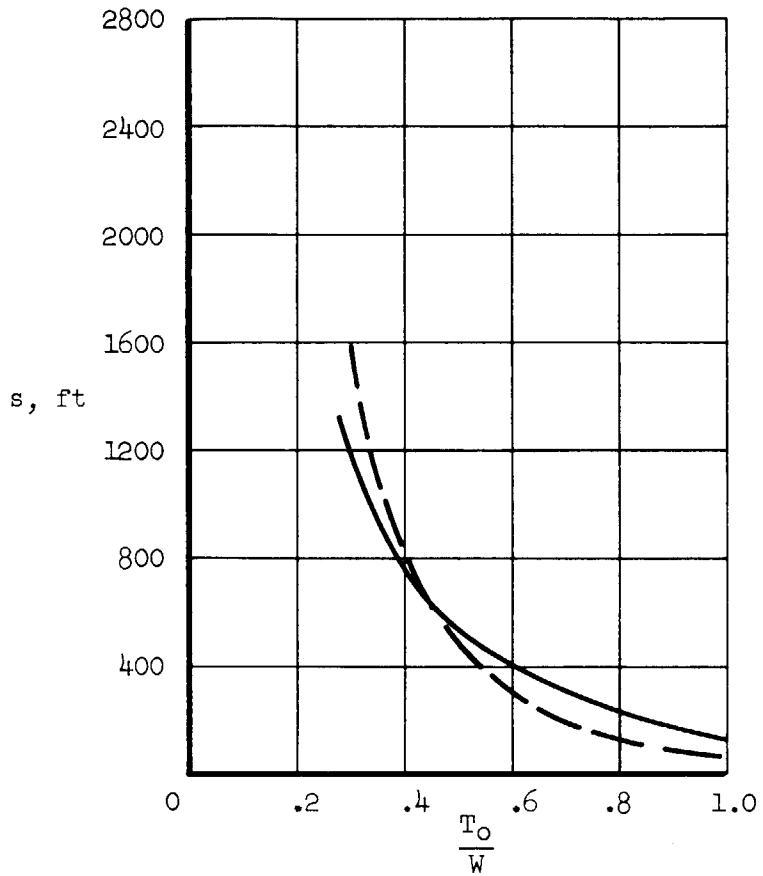

(a) Distance to take-off.

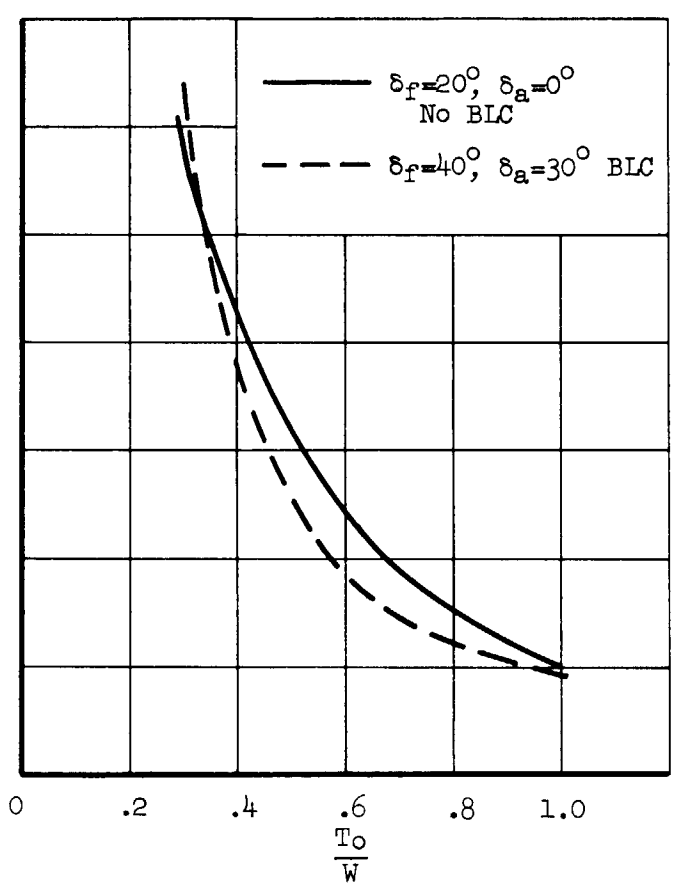

(b) Total distance to 50 feet.

Figure 9.- STOL take-off as affected by static thrust-to-weight ratio; take-off speed equal to 1.15 times the power-on stall speed; W/S = 50 lb/ft^2, μ = 0.1.

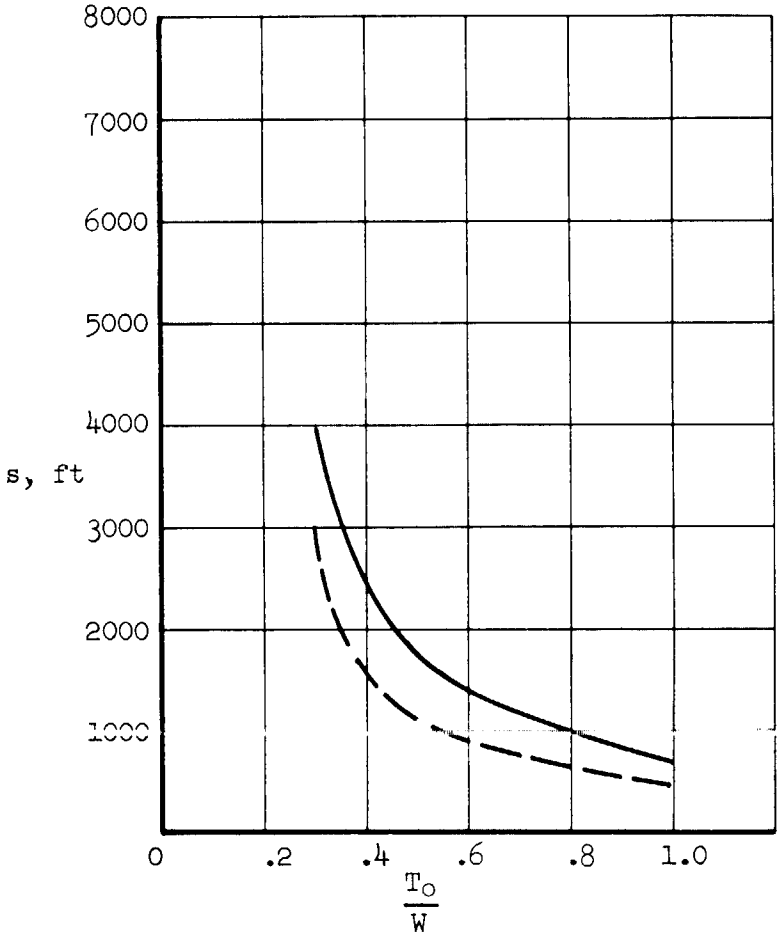

(a) Distance to take-off.

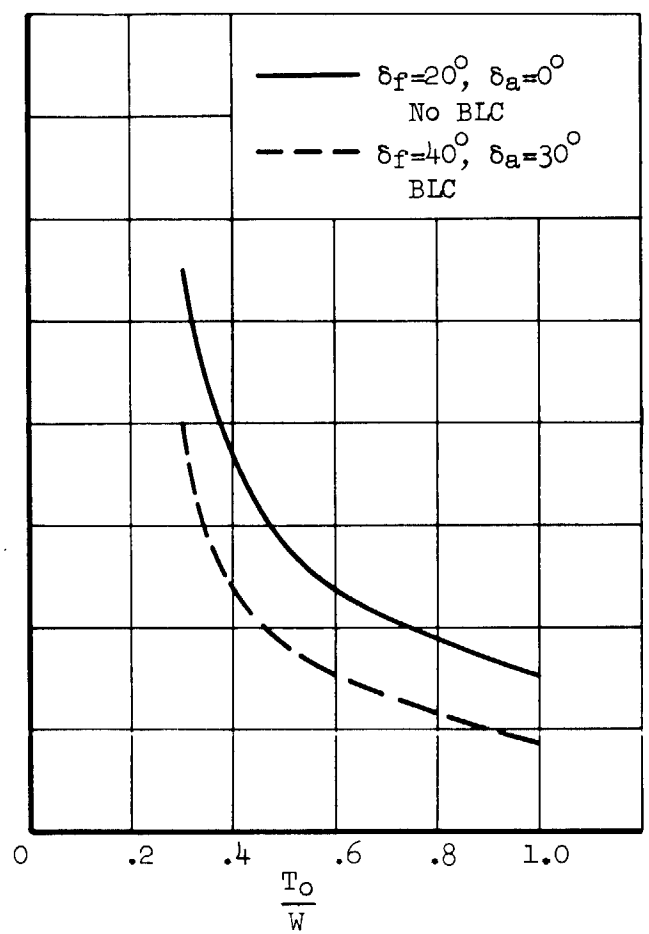

(b) Total distance to 50 feet.

Figure 10.- Conventional take-off as affected by static thrust-to-weight ratio; take-off speed equal to 1.15 times the power-off stall speed; $W/S = 50$ lb/ft^2, $\mu = 0.03$.

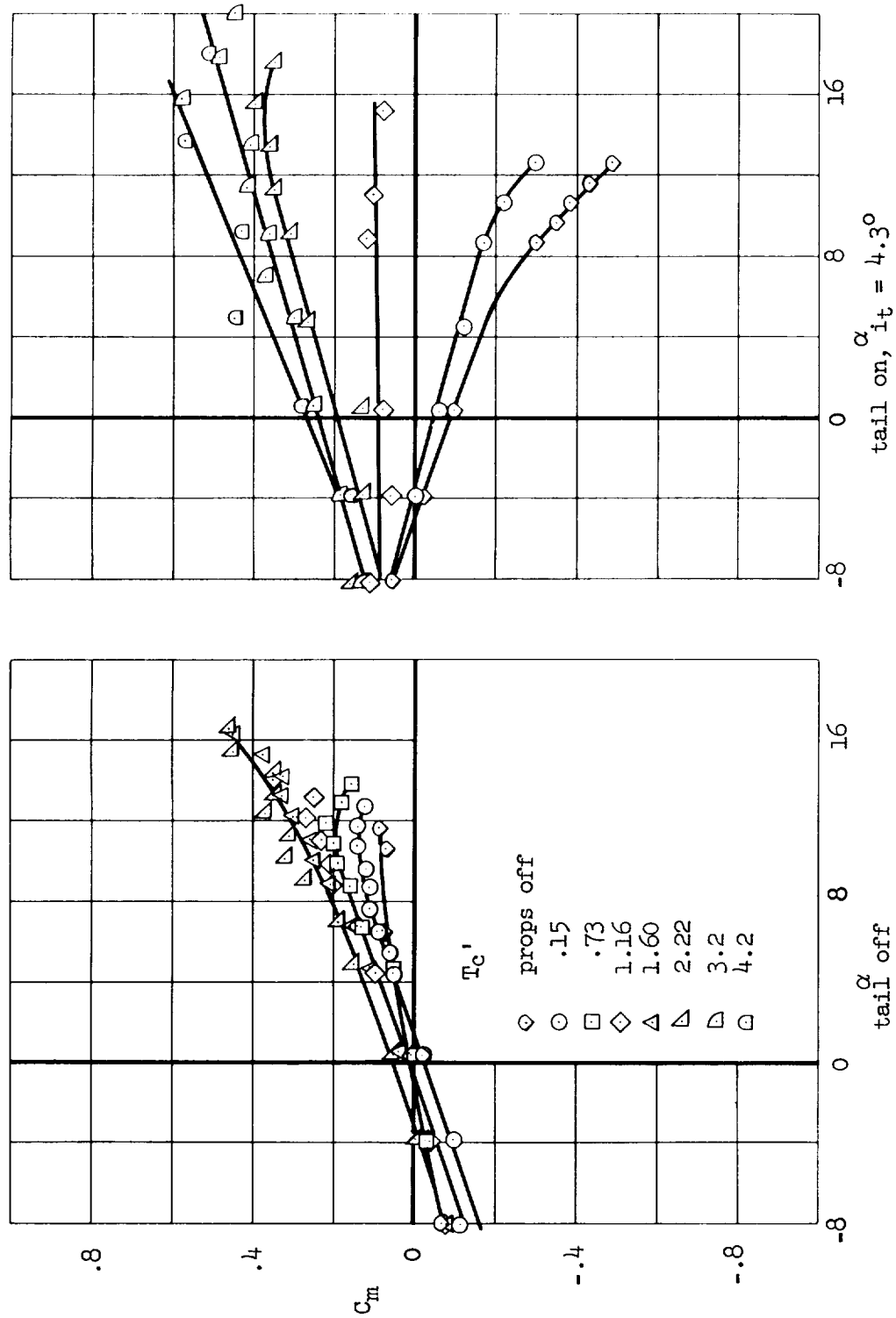

(a) $\delta_f = 0^\circ$, $\delta_a = 0^\circ$, center of gravity at $x/\bar{c} = 0.25$, $z/\bar{c} = 0$.

Figure 11.- Pitching-moment characteristics of four-propeller model.

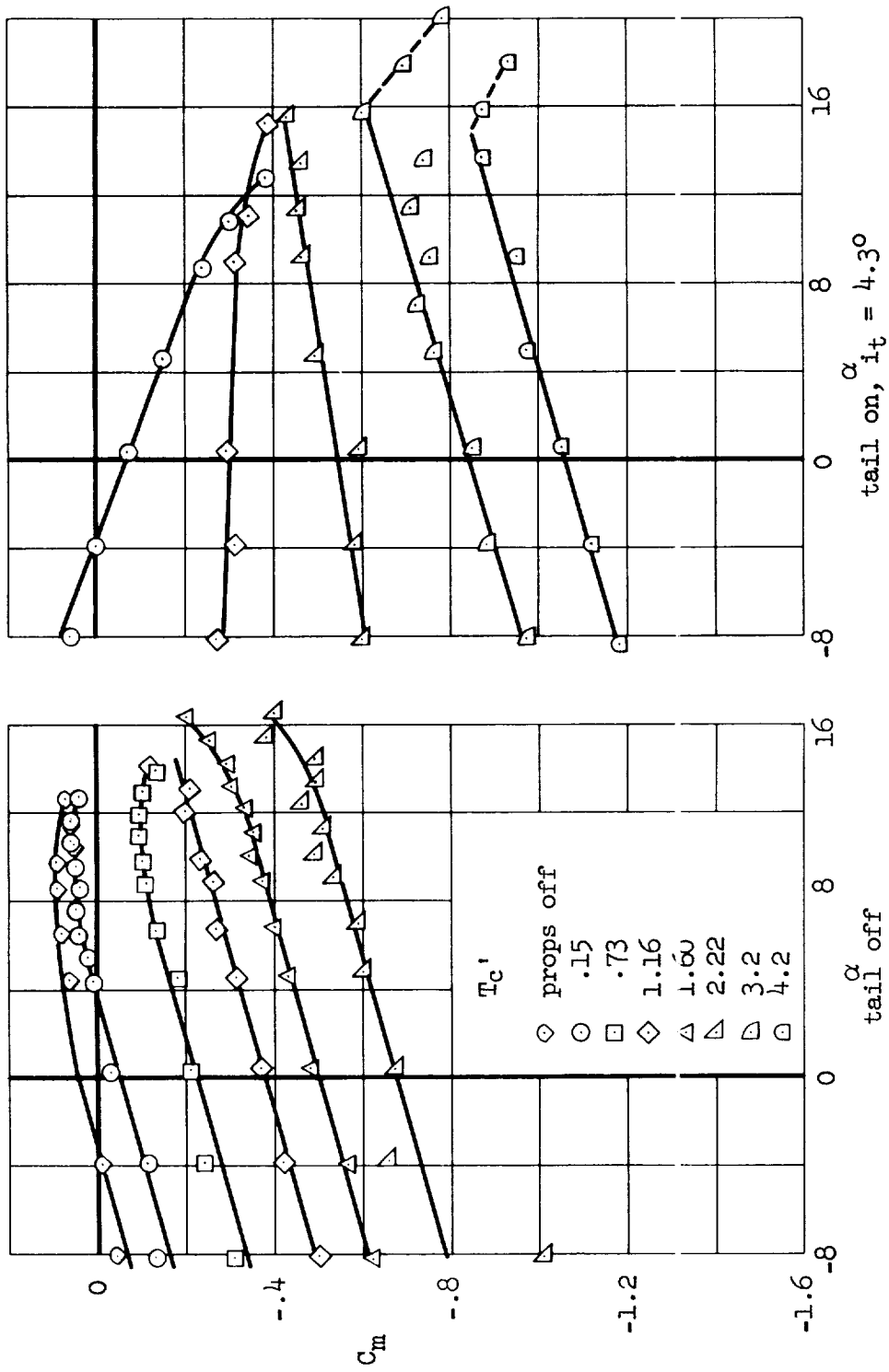

(b) $\delta_f = 0^\circ$, $\delta_a = 0^\circ$, center of gravity at $x/\bar{c} = 0.25$, $z/\bar{c} = 0.35$.

Figure 11.- Continued.

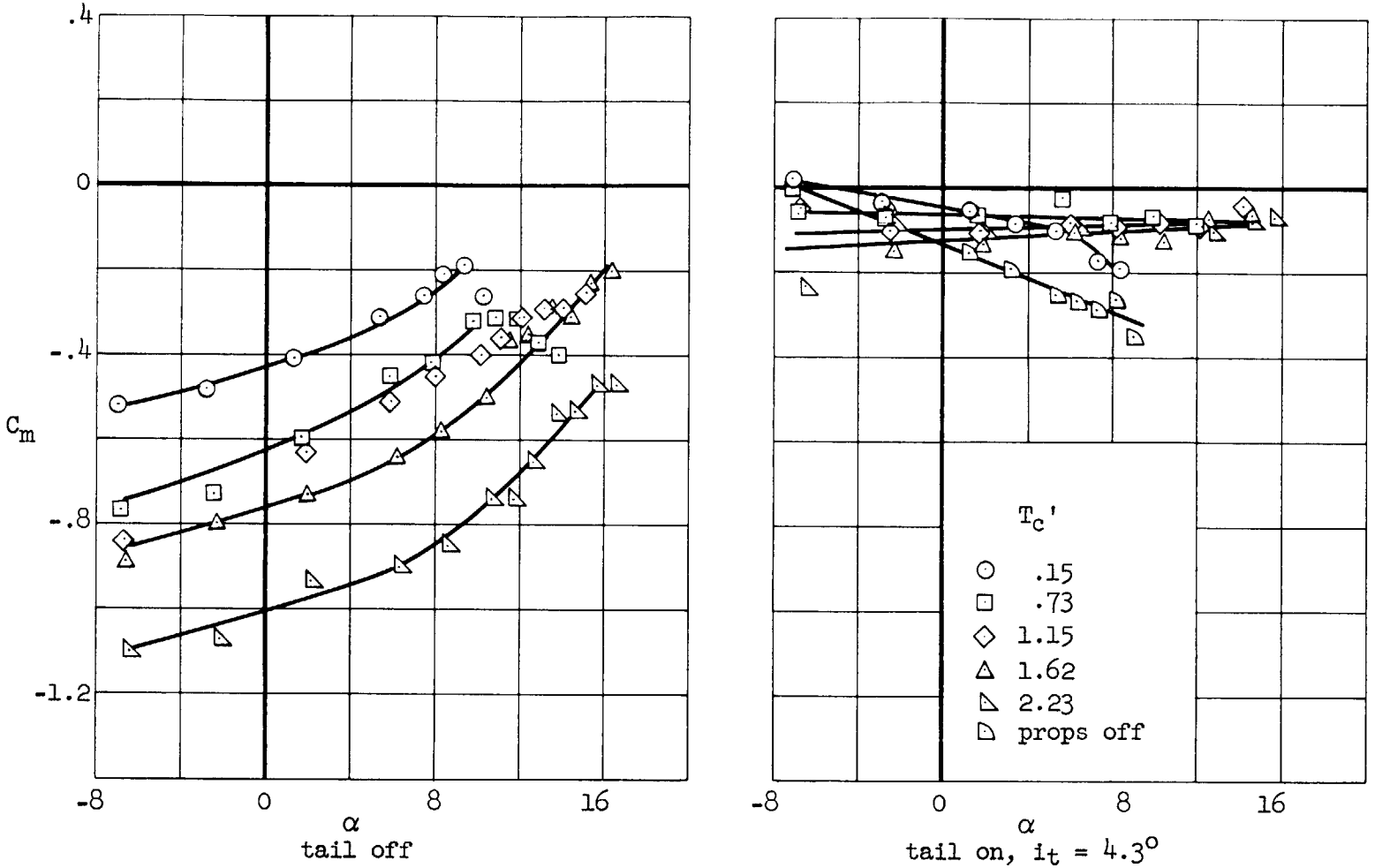

(c) $\delta_f = 60^\circ$, $\delta_a = 30^\circ$, $C_{\mu_f} = 0.035$, $C_{\mu_a} = 0.006$, center of gravity at $x/\bar{c} = 0.25$, $z/\bar{c} = 0$.

Figure 11.- Continued.

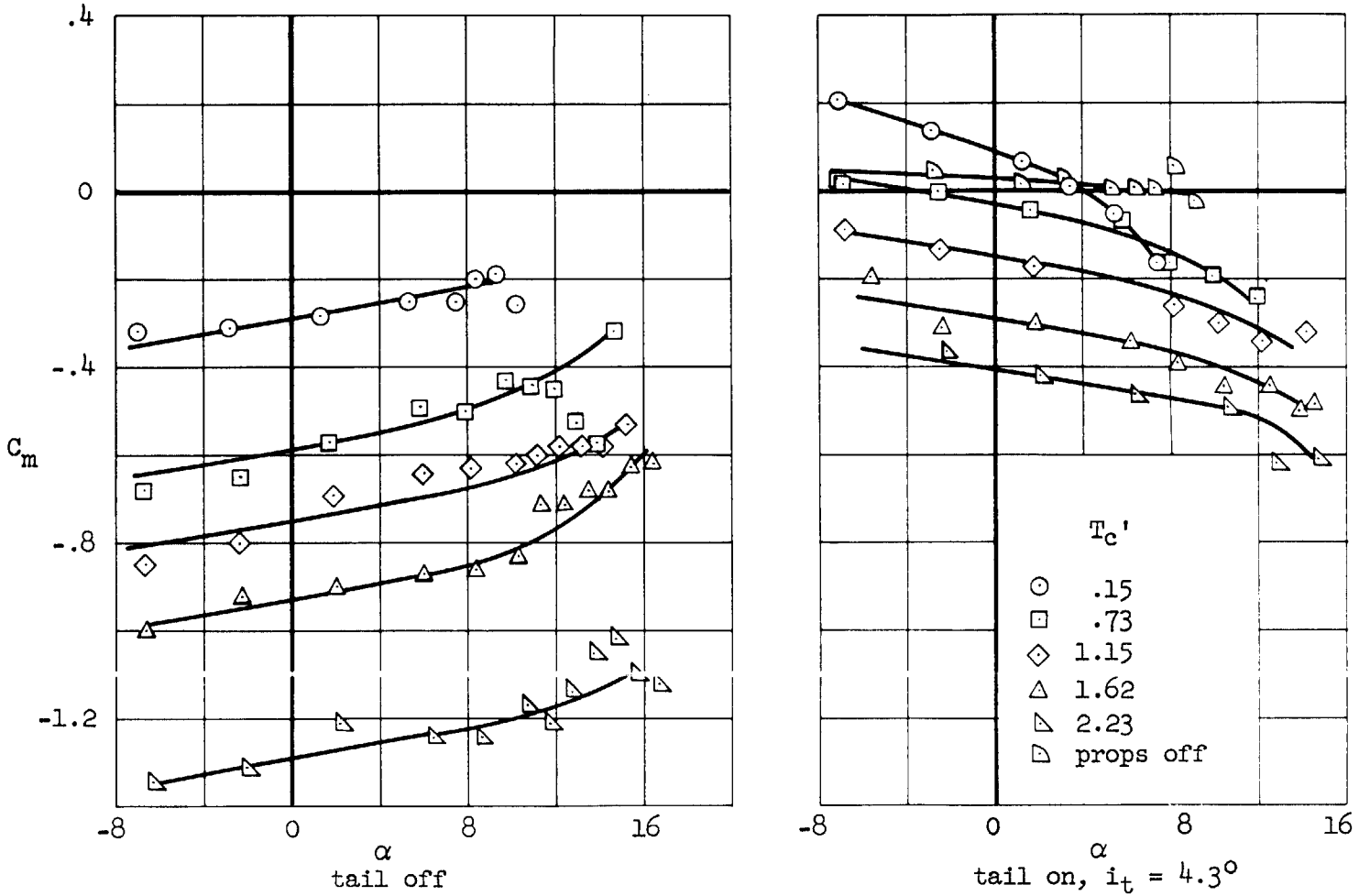

(d) $\delta_f = 60°$, $\delta_a = 30°$, $C_{\mu_f} = 0.035$, $C_{\mu_a} = 0.006$, center of gravity at $x/\bar{c} = 0.25$, $z/\bar{c} = 0.35$.

Figure 11.- Concluded.

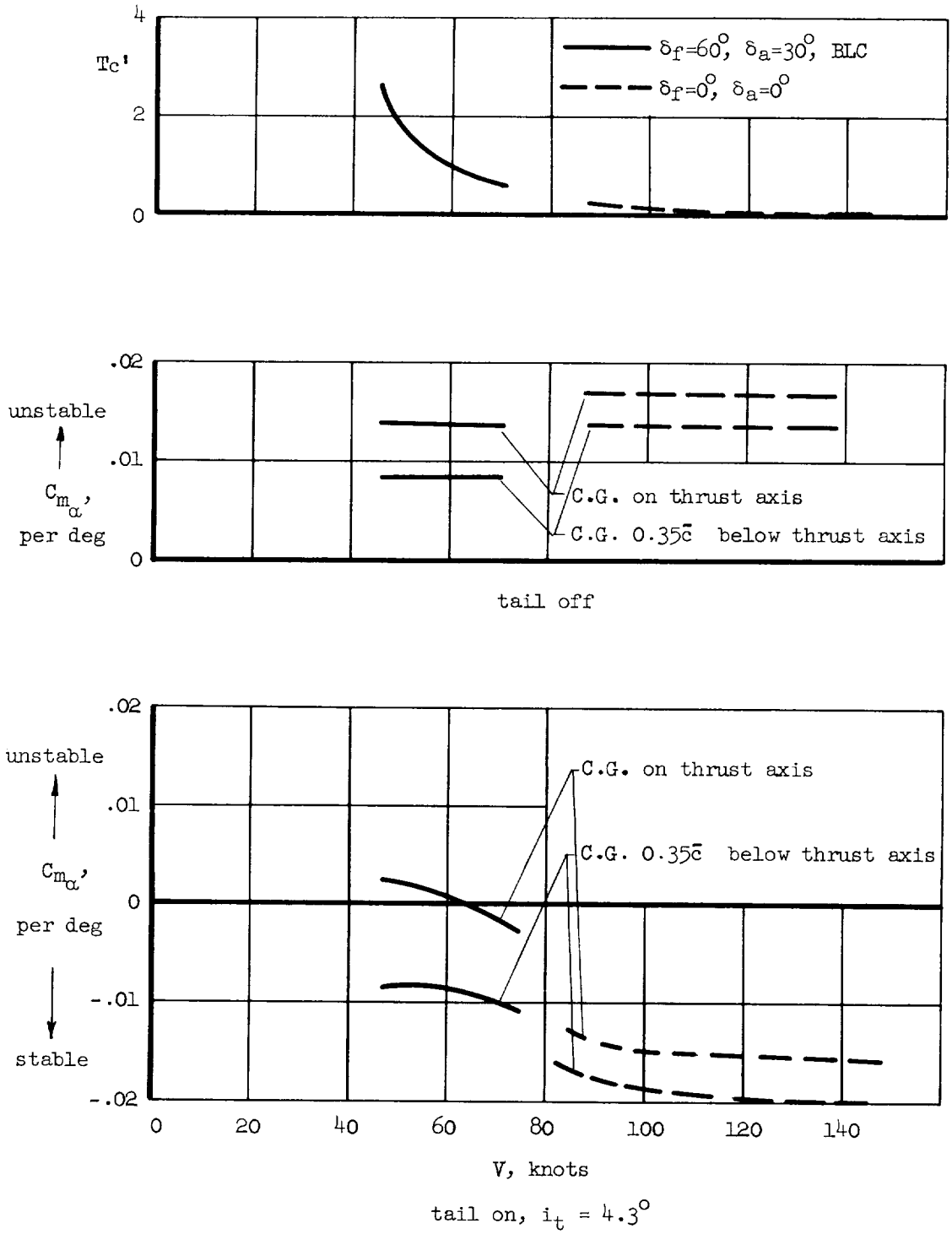

Figure 12.- Variation of attitude stability with forward velocity; level unaccelerated flight, W/S = 50 lb/ft^2, horizontal location of center of gravity at 0.25$\bar{c}$.

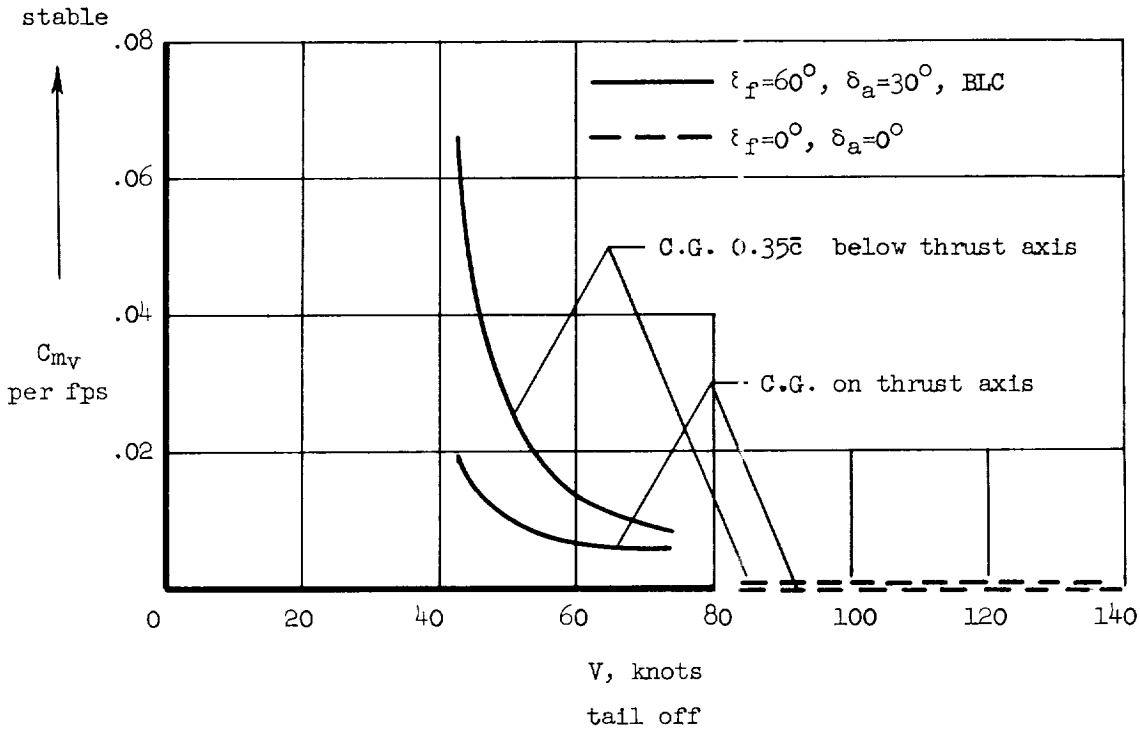

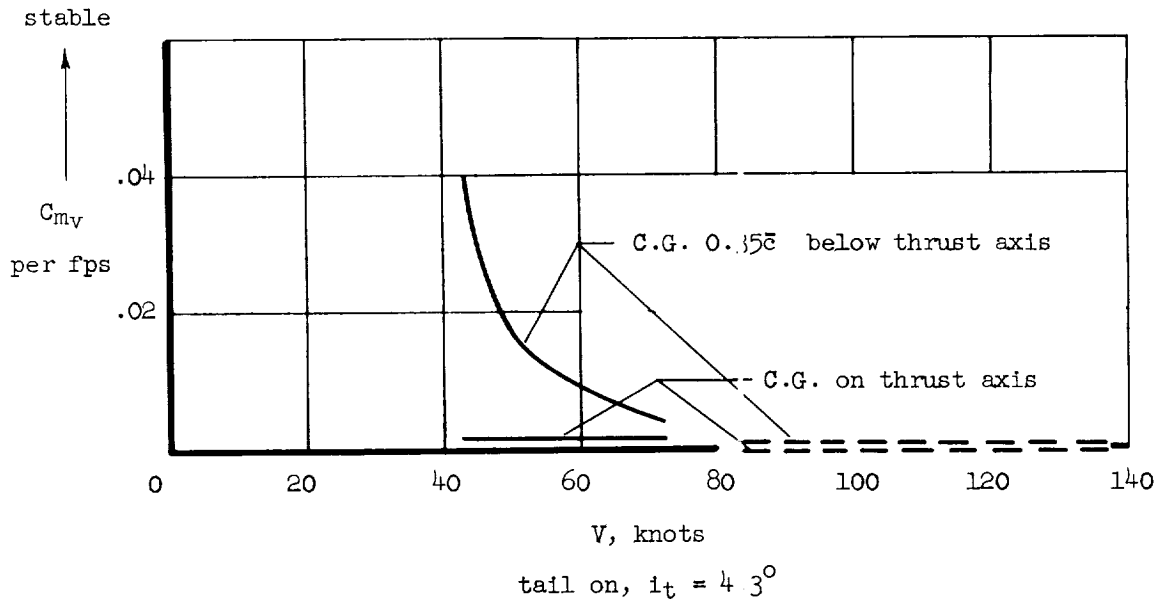

Figure 13.- Variation of speed stability with forward velocity; level unaccelerated flight, W/S = 50 lb/ft^2, horizontal location of center of gravity at 0.25$\bar{c}$.

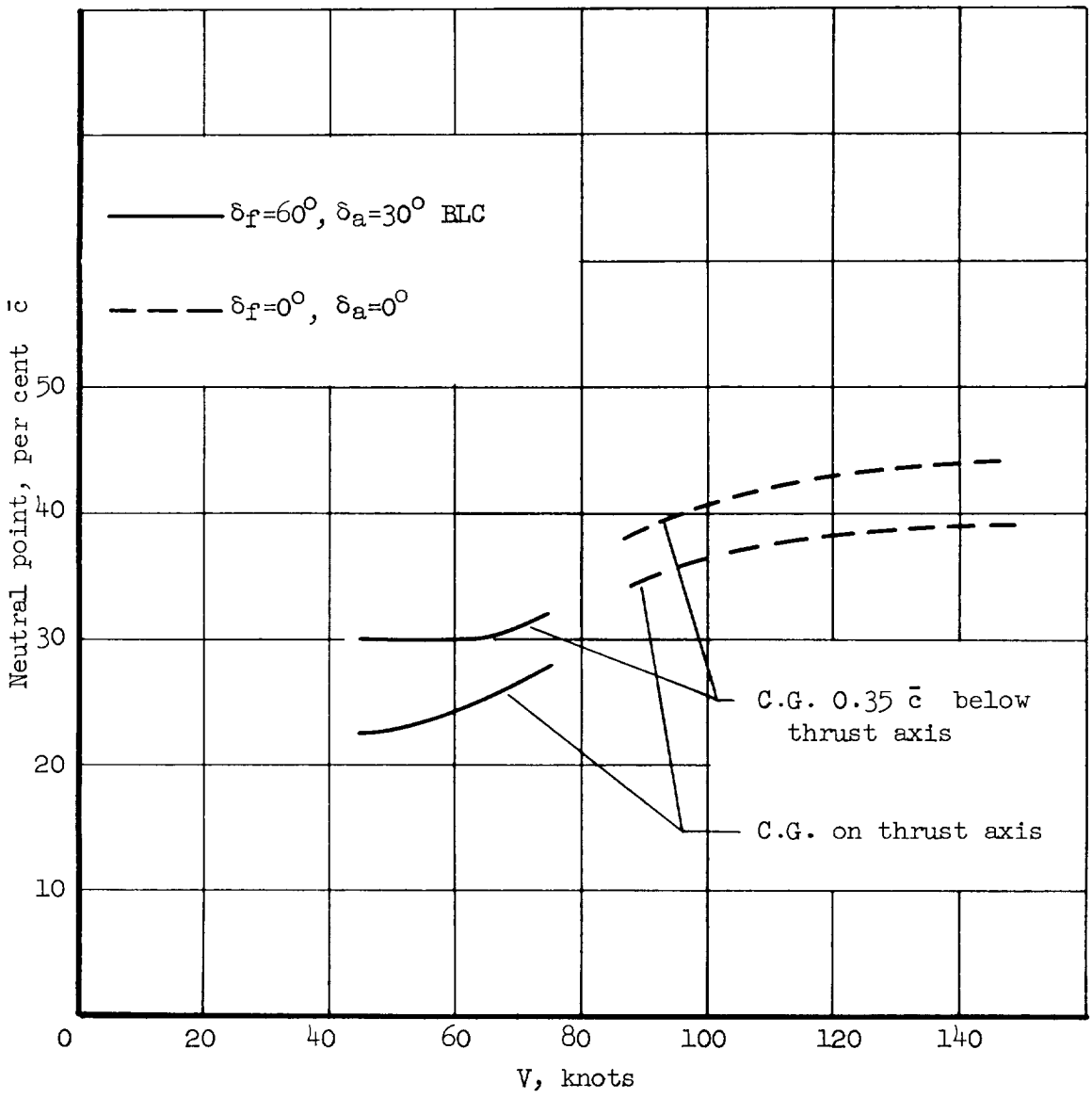

Figure 14.- Variation of neutral point with forward velocity; $W/S = 50$ lb/ft^2, $i_t = 4.3^o$, level unaccelerated flight.

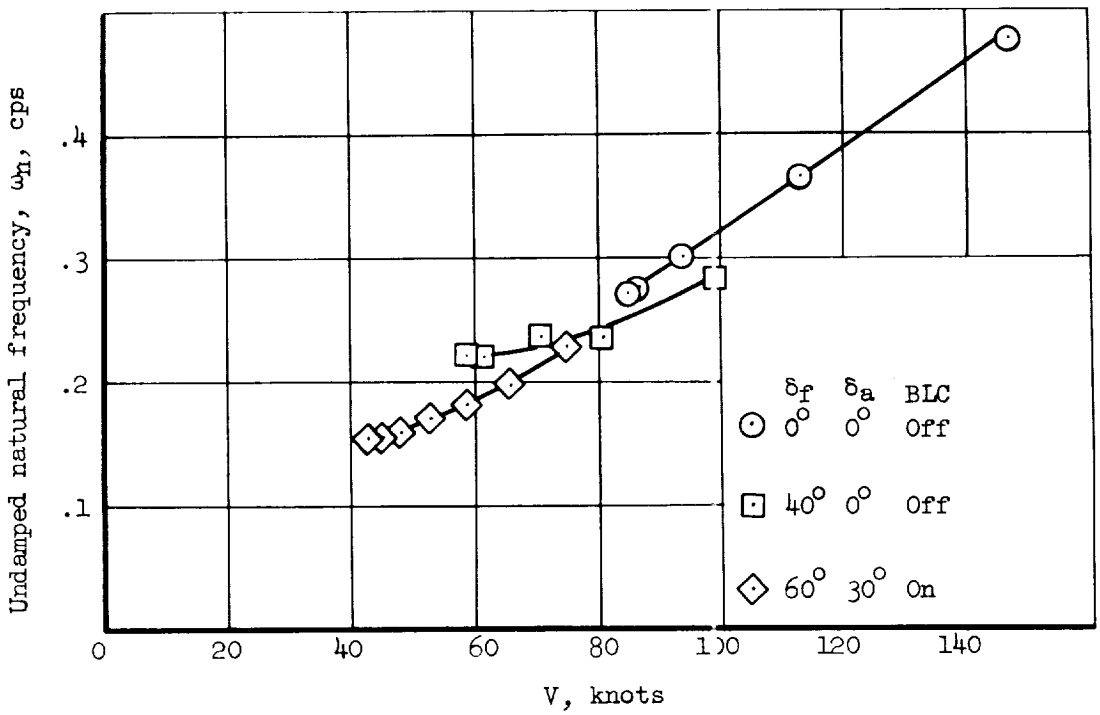

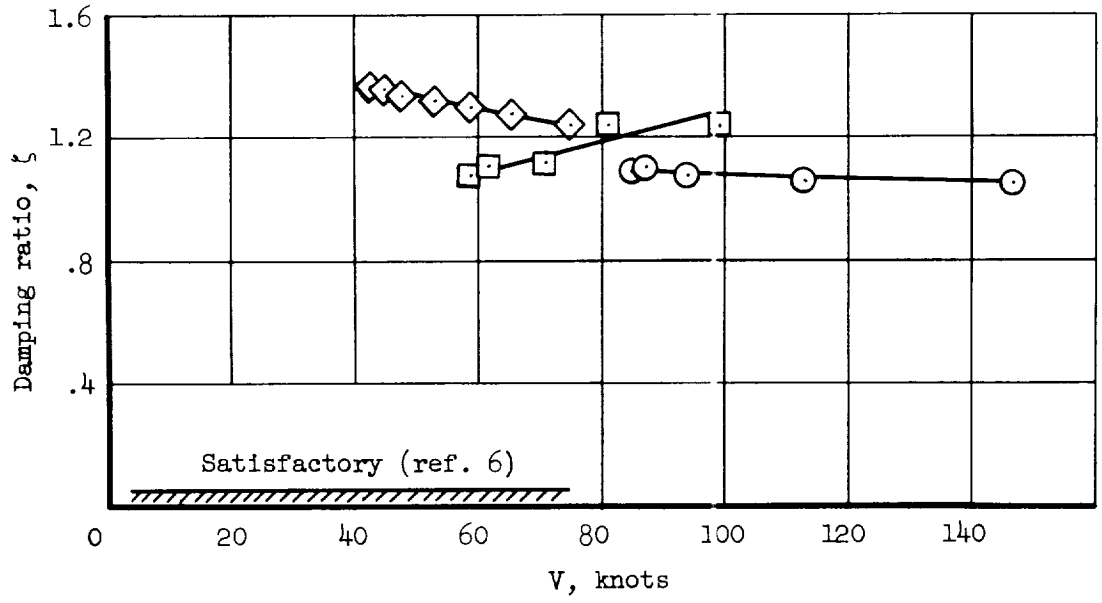

Figure 15.- Calculated dynamic short-period longitudinal characteristics; level unaccelerated flight; center of gravity located horizontally at 0.25$\bar{c}$, vertically 0.35$\bar{c}$ below thrust axis; W/S = 50 lb/ft^2.

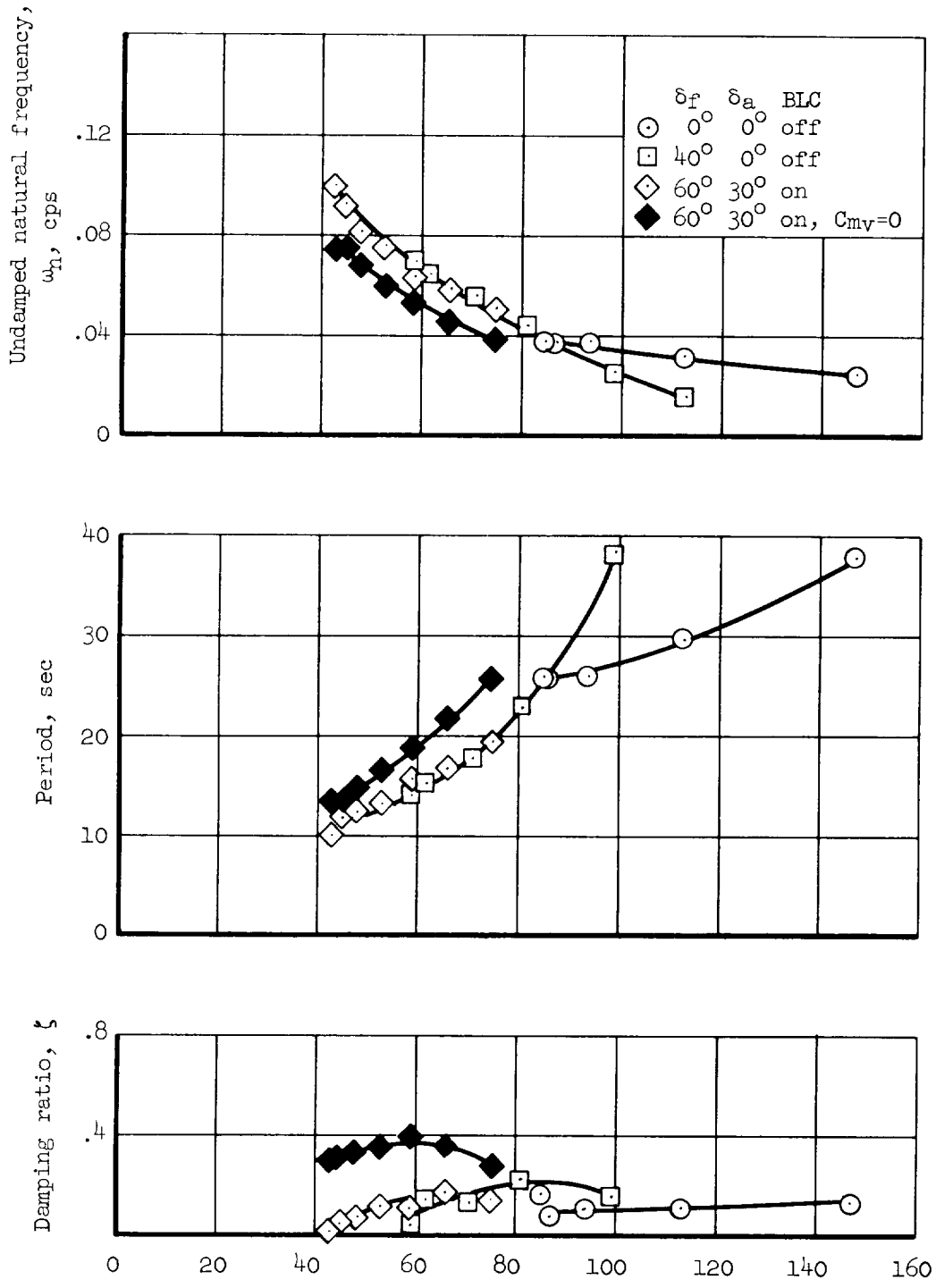

Figure 16.- Calculated dynamic phugoid longitudinal characteristics; level unaccelerated flight; center of gravity located horizontally at 0.25$\bar{c}$, vertically 0.35$\bar{c}$ below thrust axis; W/S = 50 lb/ft^2.

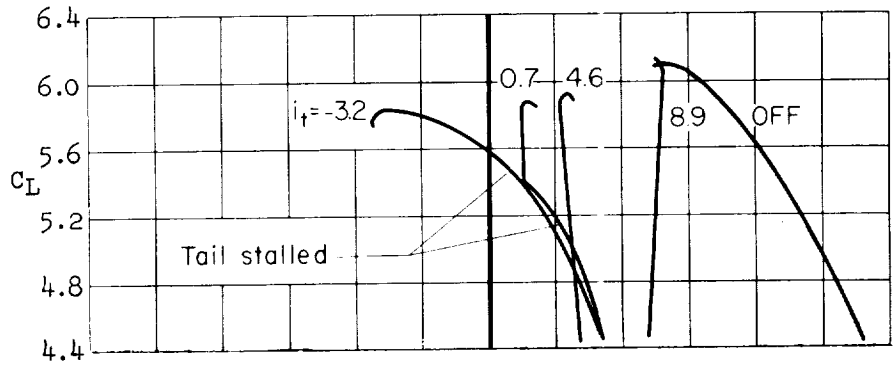

(a) Effect of tail incidence, $\delta_e = 0^\circ$, nose flap off.

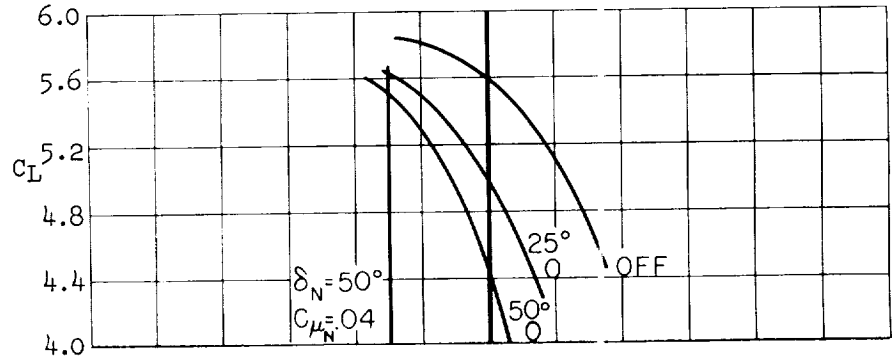

(b) Effect of nose flap and BLC, $\delta_e = 0^\circ$, $i_t = -3.2^\circ$.

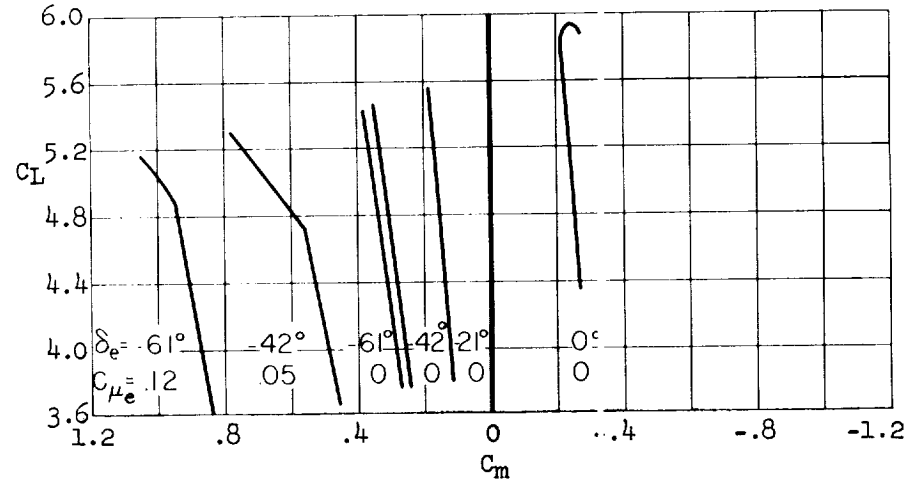

(c) Effect of elevator deflection and BLC, $i_t = 4.3^\circ$, nose flap off.

Figure 17.- Pitching-moment characteristics for various horizontal-tail configurations; $\delta_f = 80^\circ$, $\delta_a = 30^\circ$, BLC on, $T_c' = 1.15$, center of gravity located at the intersection of the thrust axis and $0.25\bar{c}$.

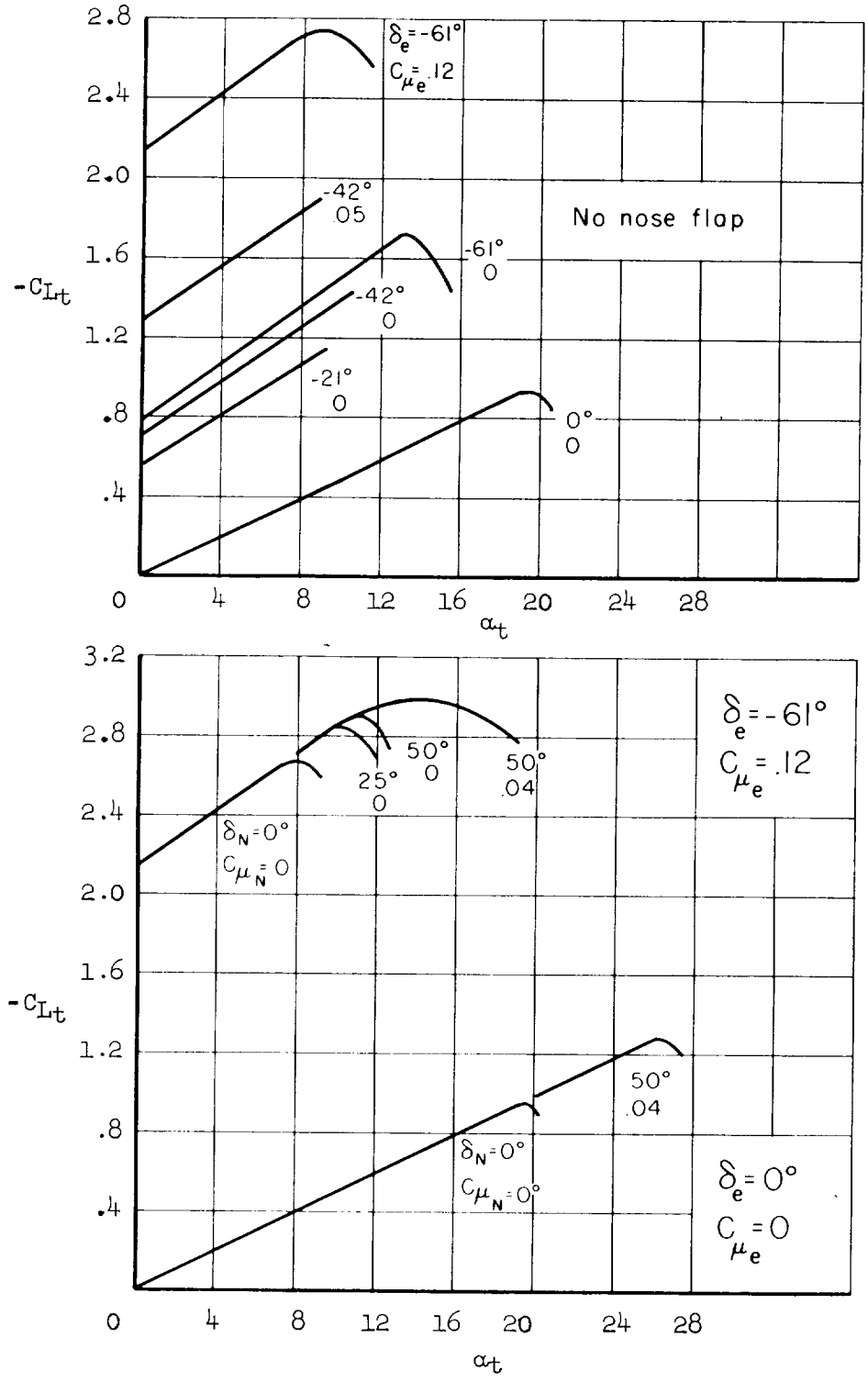

Figure 18.- Summary of horizontal-tail characteristics as affected by elevator deflection, nose flap, and BLC on elevator and nose flap.

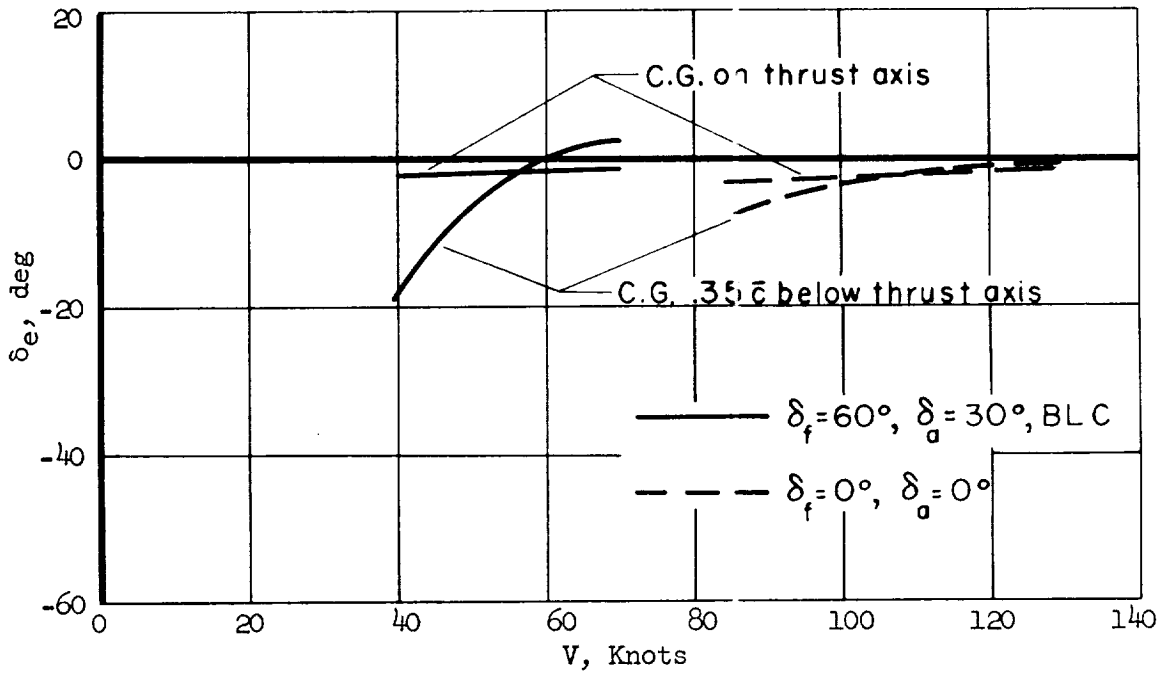

(a) Elevator deflection required to trim, $i_t = 4.3°$.

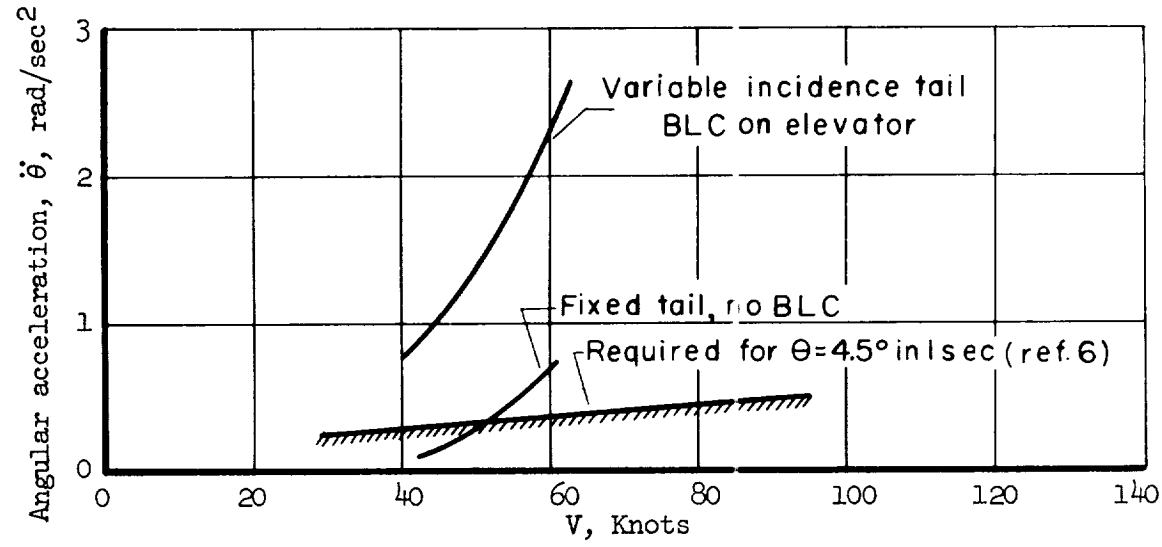

(b) Pitching acceleration for $\delta_f = 60°$, $\delta_{t_1} = 30°$, BLC on, and with center of gravity $0.35\bar{c}$ below thrust axis.

Figure 19.- Longitudinal control characteristics in level unaccelerating flight; W/S = 50 lb/ft², horizontal center of gravity at $0.25\bar{c}$.

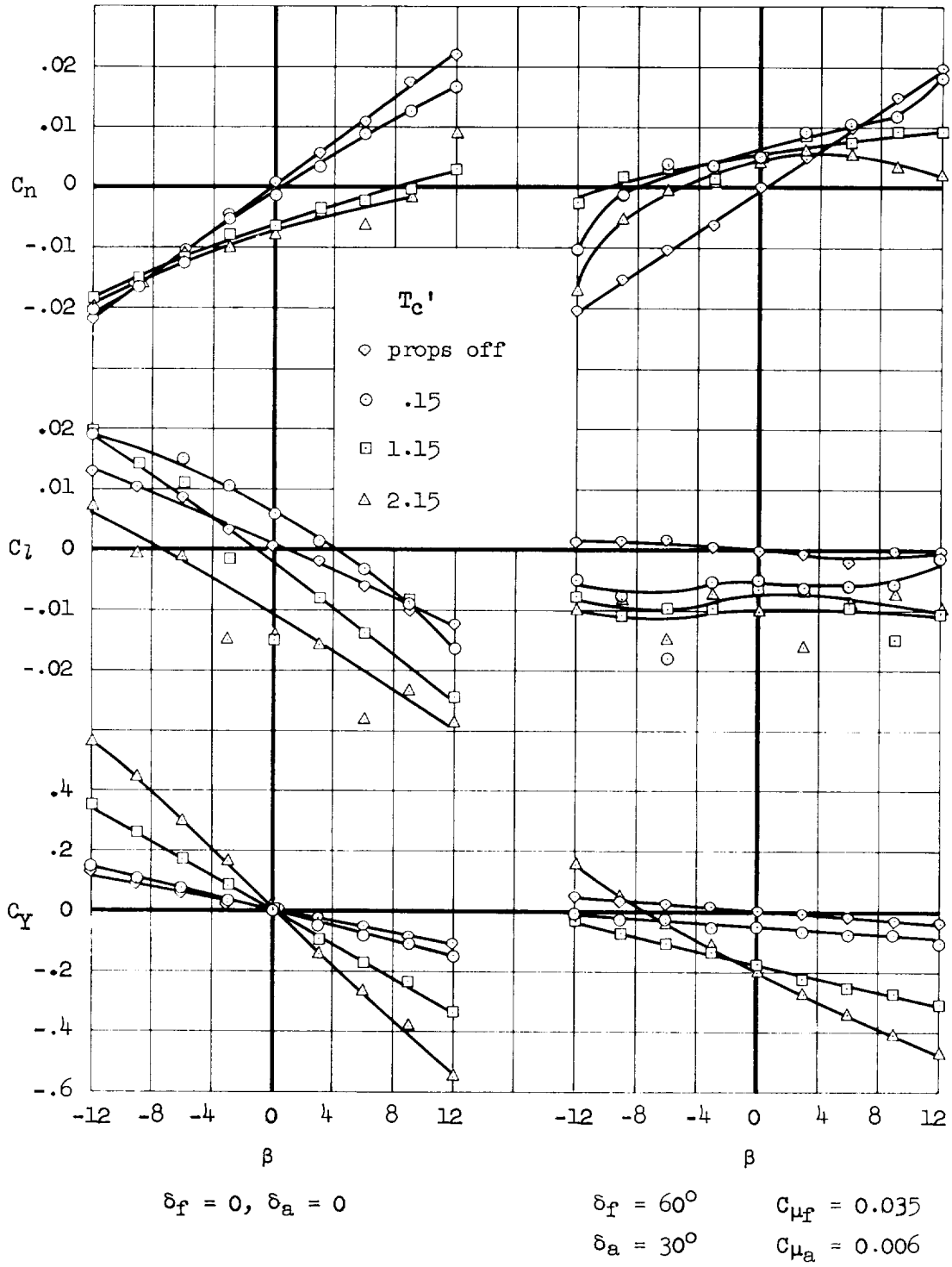

Figure 20.- Lateral and directional characteristics of four-propeller model in sideslip; vertical and horizontal tails on, $\alpha = 0°$.

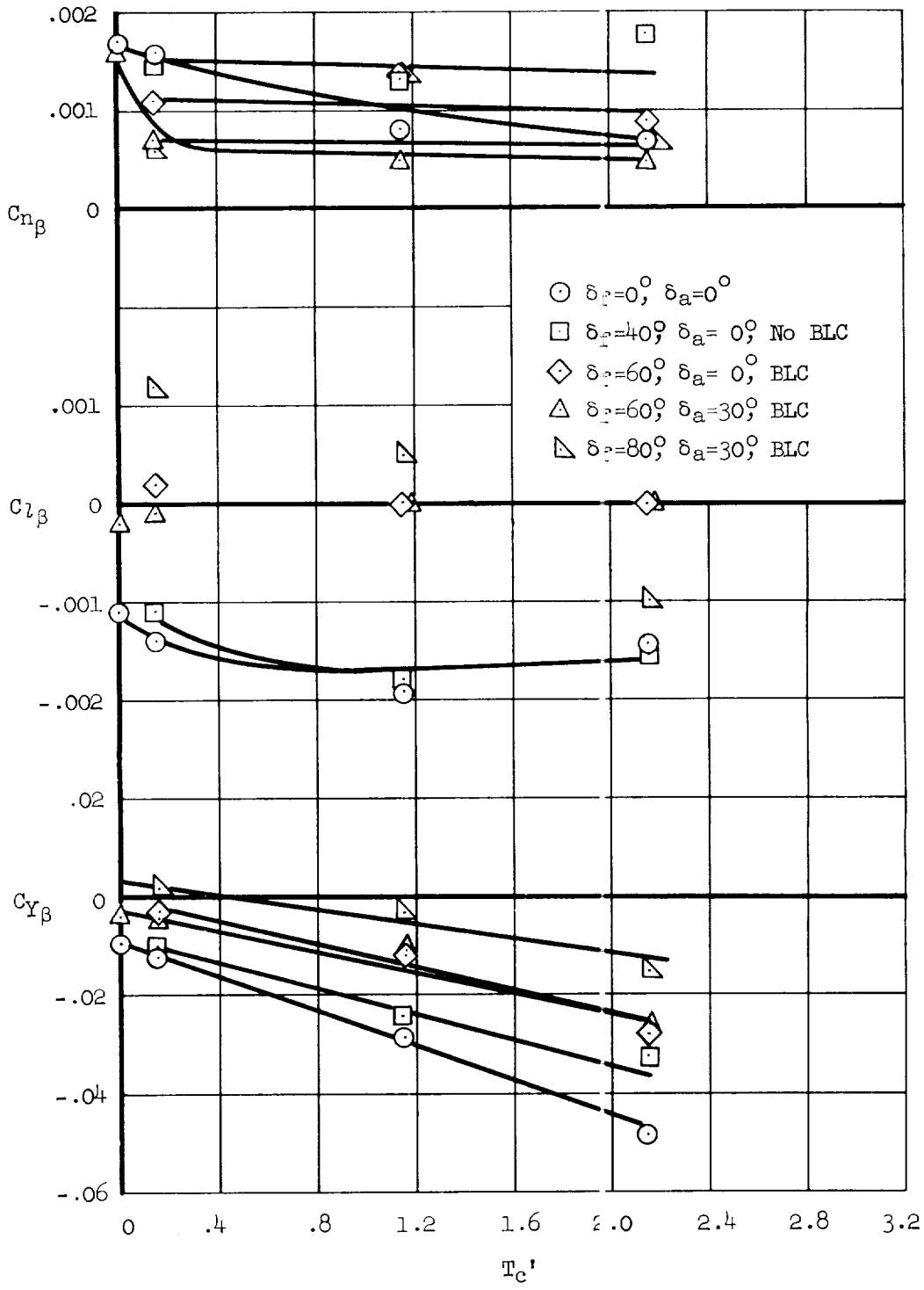

A 4 2 3

Figure 21.- Effect of thrust coefficient and flap deflection on lateral and directional stability derivatives near 0° sideslip; four-propeller model at 0° angle of attack.

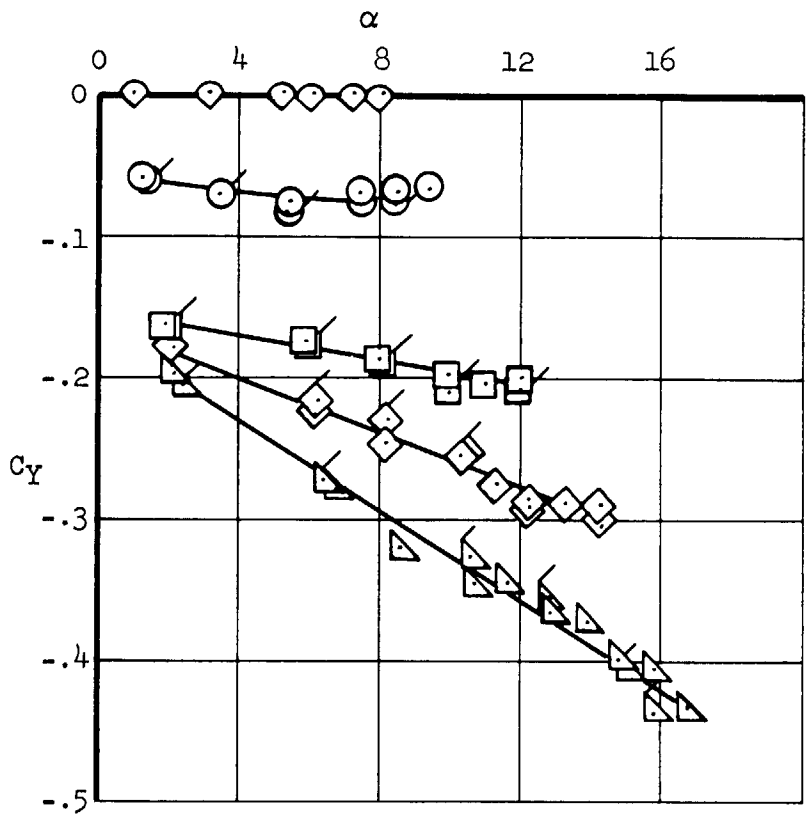

(a) Four-propeller model, diameter = 4.77 ft (ref. 4).

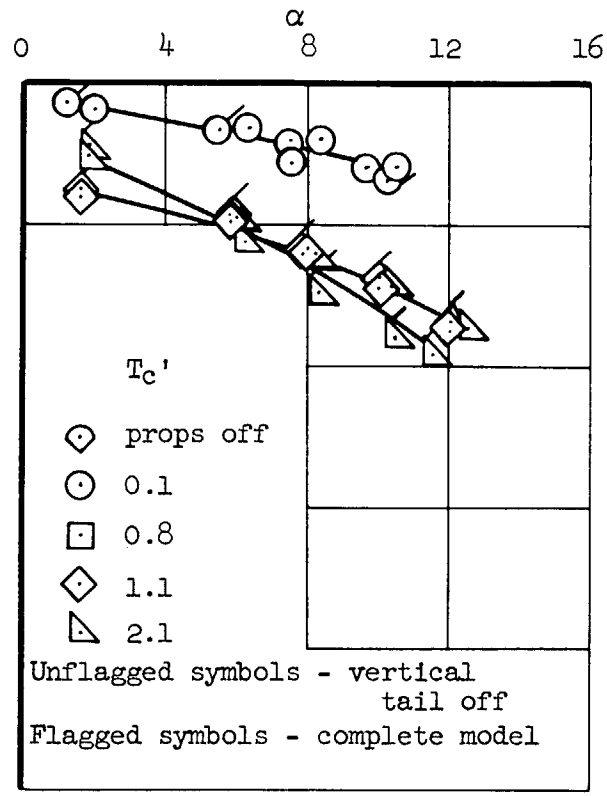

(b) Two-propeller model, diameter = 6.75 ft (ref. 2).

Figure 22.- Variation of side-force coefficient with angle of attack; $\delta_f = 60^\circ$, $\delta_a = 30^\circ$, BLC on.

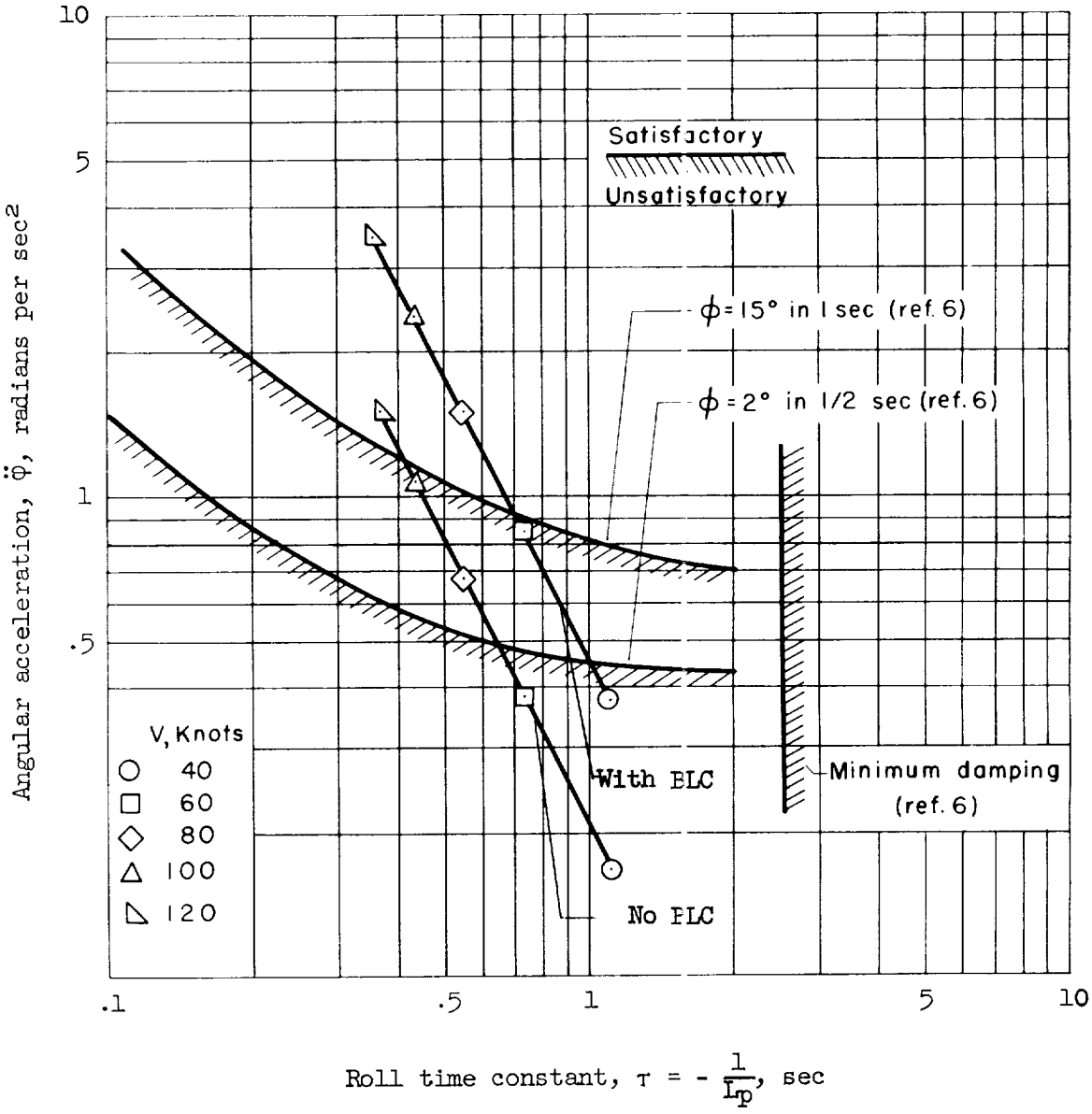

Figure 23.- Lateral control characteristics of assumed airplane with full control, W/S = 50 lb/ft^2.

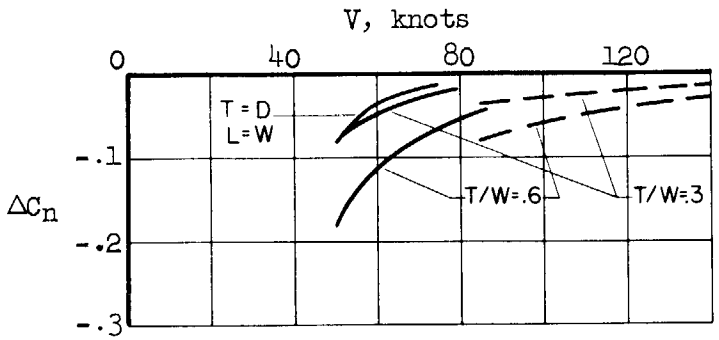

(a) Out of trim yawing-moment coefficient.

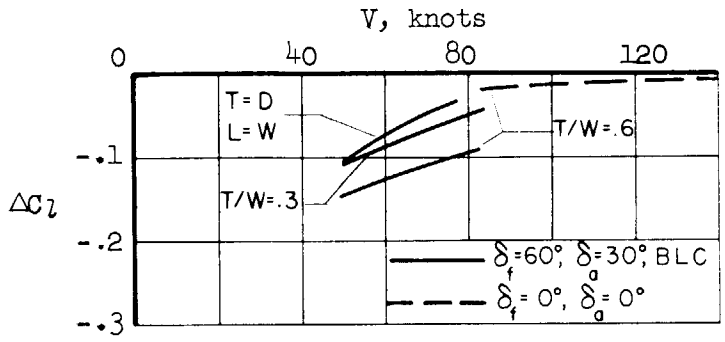

(b) Out of trim rolling-moment coefficient.

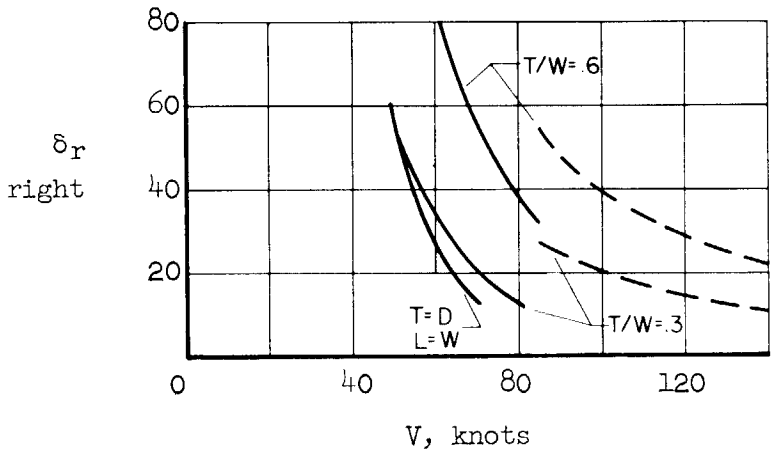

(c) Rudder deflection required for trim; BLC on rudder, $C_{n_{\delta_r}}$ = 0.00145.

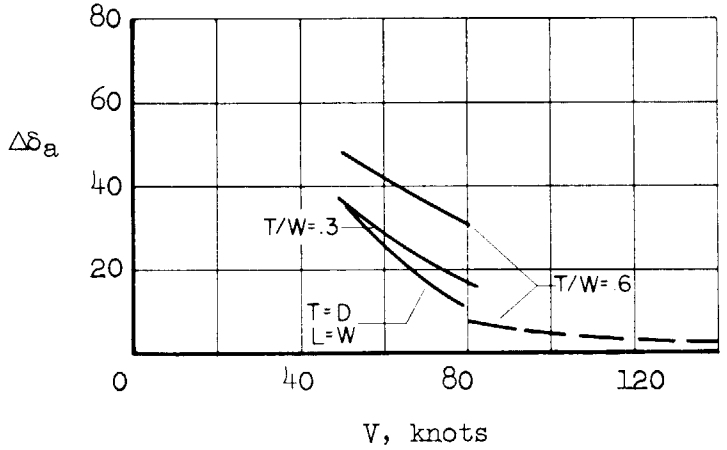

(d) Total differential aileron deflection required for trim; BLC on ailerons, $C_{l_{\delta_a}}$ = 0.0030.

Figure 24.- Lateral and directional control required with asymmetric power; four-propeller model with left outboard propeller removed; W/S = 50 lb/ft^2.

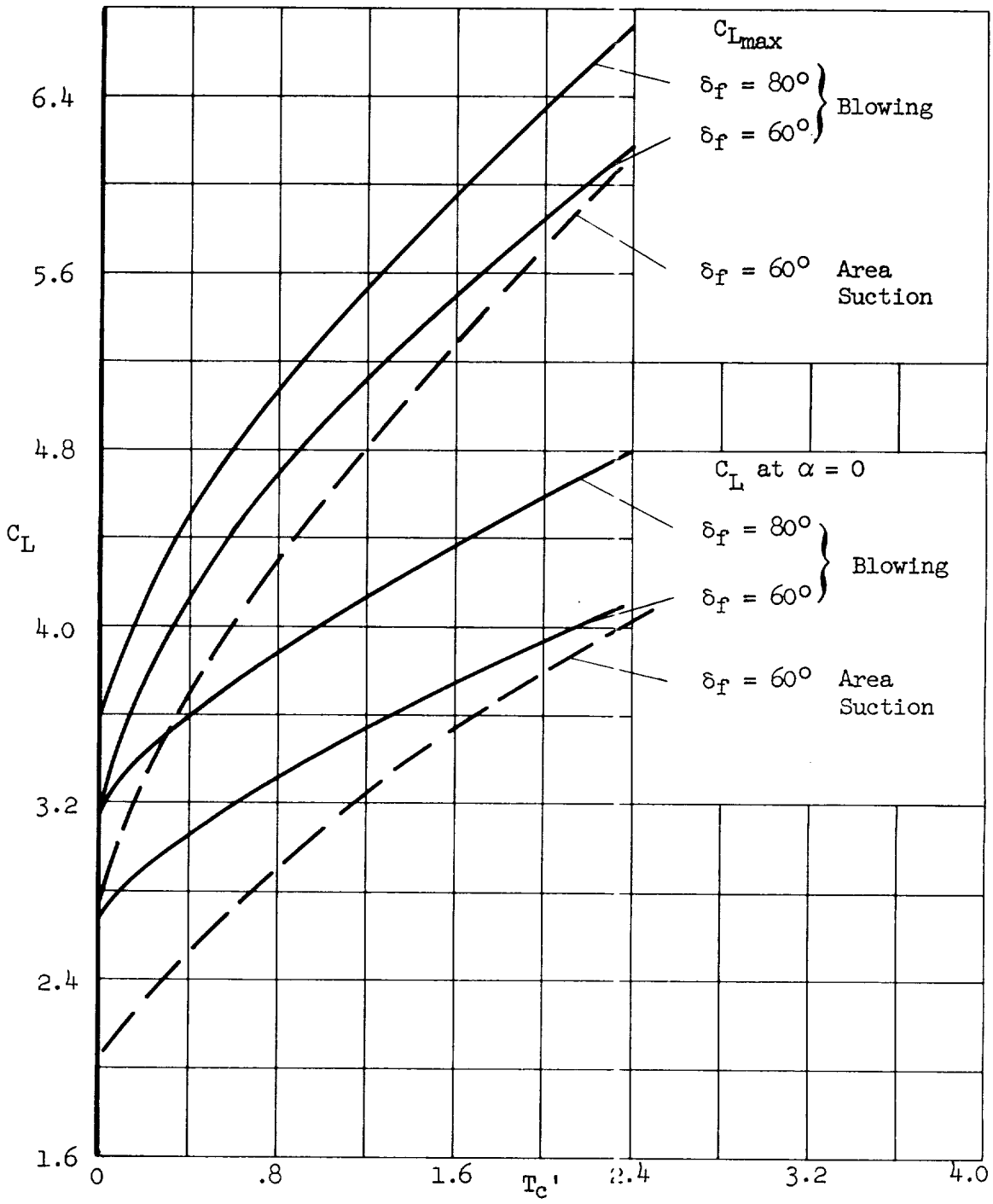

A423

Figure 25.- Comparison of lift obtained with area suction and with blowing; flow quantities near critical values; two-propeller model (refs. 2 and 3).

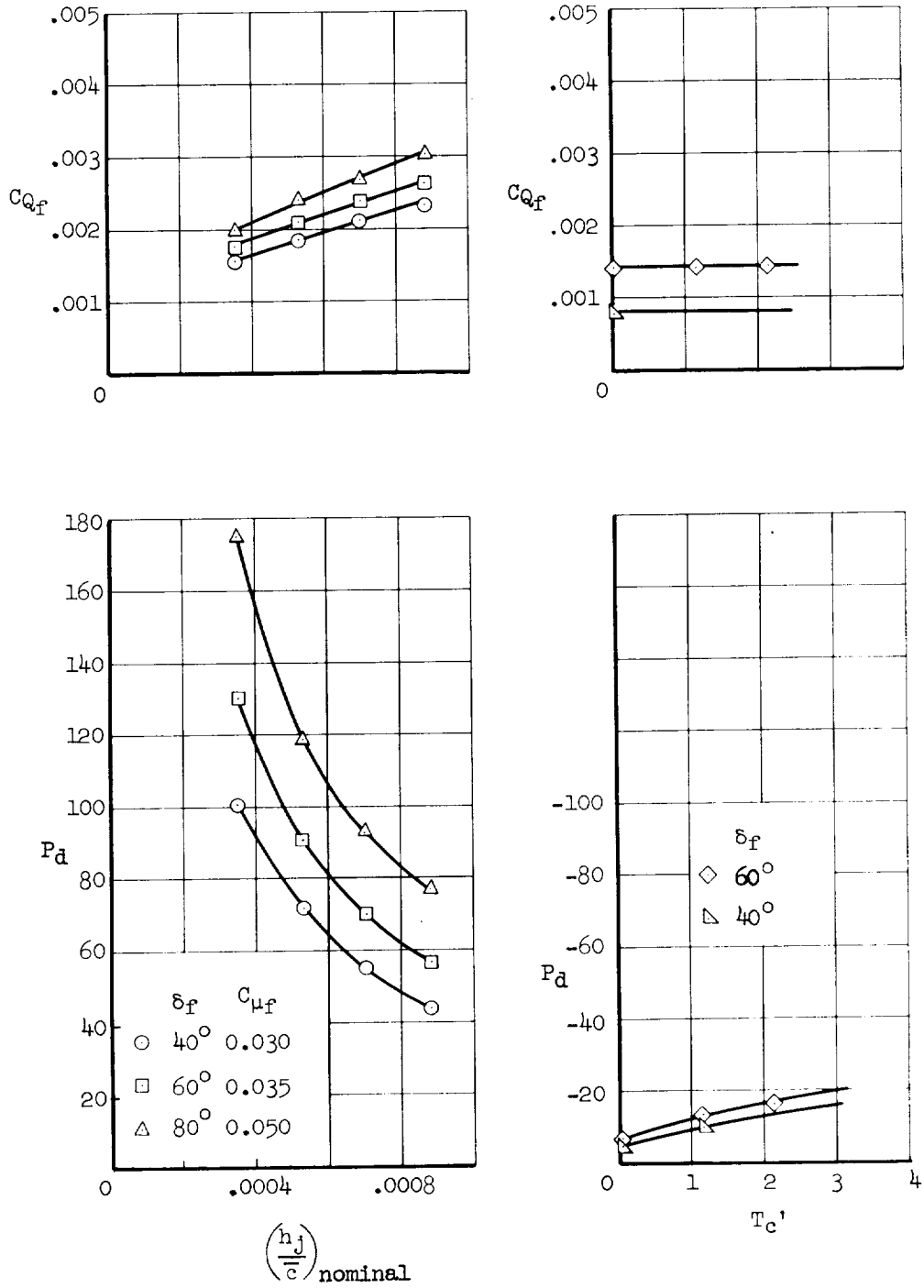

(a) Blowing; critical flow quantities invariant with T_c'.

(b) Area suction; optimum chordwise extent.

Figure 26.- Comparison of flap pumping requirements at critical values for blowing and area suction.